LUT UNIVERSITY
LUT School of Energy Systems
LUT Mechanical Engineering

Kalle-Matti Rekola

UTILIZATION OF METAL SANDWICH PANEL AS LOAD-BEARING STRUCTURE

Examiners: Professor Timo Björk
Lic. Sc. (Tech.) Roope Eskola

TIIVISTELMÄ

LUT-Yliopisto
LUT School of Energy Systems
LUT Kone

Kalle-Matti Rekola

Utilization of metal sandwich panel as load-bearing structure

Diplomityö

2020

69 sivua, 56 kuvaa, 6 taulukkoa ja 7 liitettä

Tarkastajat: Professori Timo Björk
TkL Roope Eskola

Hakusanat: Kerroslevyrakenne, kennorakenne, teräs, FE-analyysi, analyyttinen laskenta

Tämän diplomityön tavoitteena oli suunnitella kuormaa kantava teräskennorakenne sekä liitoselementit, jotka soveltuva korotettuihin lämpötiloihin. Kennoon kohdistuvat rasitukset laskettiin lujuusopin perusteita ja palkkiteoriaa käyttäen. Suunnittelussa sovellettiin kennorakenteisiin liittyvää teoriaa sekä Eurokoodi 3:en liittyvää levyteoriaa. Analyyttisen laskennan lisäksi kennorakenne tutkittiin elementtimenetelmällä.

Kennon ydinprofiiliksi valikoitui kokoonpanon kannalta valmistusystävällinen V-ydin. Kennon poikkileikkauksen mitoitukseen kehitettiin analyyttiseen laskentaan perustuva Excel VBA -ratkaisija. Ratkaisija noudatti poikkileikkausluokka 3:n levykenttien hoikkuussuhteita. Ratkaisun perusteella tehdyt FE-mallit korreloivat riittävällä tarkkuudella analyyttisesti lasketun kennon taipuman kanssa. FE-mallin avulla simuloitiin kennon värähtelymuotoja sekä kestävyyttä poikittaista maanjäristyskuormaa vastaan.

Stabiliteettitarkasteluissa kenno todettiin turvalliseksi. Kennorakenteen painoa voidaan keventää poikkileikkausluokan muutoksella. Ydinten väliä kasvattamalla myös valmistuskustannuksissa olisi mahdollista saavuttaa säästöä. Excel-ratkaisija todettiin hyväksi työvälineeksi, joka on helposti muokattavissa erilaisiin optimointitarpeisiin.

ABSTRACT

LUT University
LUT School of Energy Systems
LUT Mechanical Engineering

Kalle-Matti Rekola

Utilization of metal sandwich panel as load-bearing structure

Master's thesis

2020

69 pages, 56 figures, 6 tables and 7 appendices

Examiners: Professor Timo Björk
Lic. Sc. (Tech.) Roope Eskola

Keywords: Sandwich panel, cell structure, steel, FE-analysis, analytical calculation

The aim of this thesis was to design a load-bearing steel sandwich structure and connecting elements for elevated temperatures. The loads of the panel were calculated based on strength of material, using beam theory. The theory of cellular structures and the plate theory of Eurocode 3 were applied in the design. In addition to analytical calculation, the cell structure was investigated by the elemental method.

An assembly-friendly V-type core was chosen for the core profile of the cell. An Excel VBA solver, based on analytical calculation, was developed for dimensioning the cross-section of the cell. The solver followed cross-section class 3 slenderness ratios of plate fields. Based on the solution, the created FE models correlated with sufficient accuracy with the analytical deflection. The FE model was used to simulate cell vibration modes and resistance to lateral seismic loads.

Based on stability analyses, the cell was found to be safe. The weight of the cell structure can be reduced by changing the cross-section class. By increasing the spacing between cores, savings in manufacturing costs could also be achieved. The Excel solver was found to be a good tool that can be easily customized for different optimization needs.

ACKNOWLEDGEMENTS

I want to express my special thanks to Raute Oyj R&D manager Roope Eskola for this interesting and challenging subject. I want to express my special thanks also to professor Timo Björk for his expert comments and work during the M.Sc studies. I express my thanks also to Raute Oyj R&D colleagues for co-operative and pleasant working atmosphere.

I feel most grateful to my friends and family for the support during this five-year experience. Hard work, support and encourage have led to this ceremonial moment of graduation.

Kalle-Matti Rekola
Nastola 29.4.2020

TABLE OF CONTENTS

LIST OF SYMBOLS AND ABBREVIATIONS

α	Coefficient for relevant category of cold formed profile
α_0	Factor for effective width calculation
β	Reduction factor for effective width
β_v	Variable related to cold formed profile effective bearing length definition
γ_F	Partial safety factor for load
γ_M	Partial safety factor for material
ε	Ratio of yield strength
η	Factor for strain hardening
κ	Factor for effective width calculation
ξ	Distance ratio
σ_{cr}	Critical buckling stress [MPa]
σ_E	Euler buckling stress [MPa]
σ	Stress [MPa]
τ_{cr}	Critical buckling stress [MPa]
ψ	Ratio of tensile and compressive stress
ω_n	Natural angular velocity [rad/s]
a	Length of cross-section or throat thickness of weld [mm]
A	Area [mm^2]
b	Width of cross-section [mm]
b_1	Distance between cores [m]
b_0	Width of flange [mm]
b_{eff}	Effective width of flange [mm]
c	Width of plate field [mm]
c_1	Height of the load [m]
E	Young's modulus [MPa]
e	Distance between neutral axis and flange [mm]
F	Load [N]
f_u	Ultimate strength of material [MPa]
f_y	Yield strength of material [MPa]
f_{yd}	Design yield strength [MPa]

g	Gravity [m/s^2]
h, H	Height of cross-section [mm]
I	Second moment area of cross-section [mm^4]
k	Spring constant [N/m]
k_w	Auxiliary variable in face sheet dimensioning
k_θ	Temperature-dependent reduction factor
k_σ	Buckling factor
k_τ	Buckling factor
L	Span between supports
L_a	Effective bearing length of the category of cold formed profile [mm]
L_e	Length between zero bending moment points [mm]
L_w	Effective length of fillet weld [mm]
M	Bending moment [Nmm]
m	Number of buckling half waves
m_1	Mass [kg]
m_2	Auxiliary variable in face sheet dimensioning
p	Surface pressure [kPa]
r	Radius [mm]
r_i	Distance between neutral axis and area center of gravity [mm]
$R_{w,Rd}$	Local transverse resistance of web [N]
$S_{a.d}$	Design spectrum
S_s	Length of stiff bearing [mm]
T	Natural period [s]
t	Thickness [mm]
u	Displacement [mm]
v	Poisson's ratio
V_{ed}	Transverse shear force [N]
W	Section modulus [mm^3]
x	Displacement [mm]
z_0	Z-coordinate of center of gravity

PGA	Peak ground acceleration

Δ	Range

1 INTRODUCTION

Raute is a global market leader in business area of providing technologies in plywood and LVL industries. Approximately half of the LVL manufactured worldwide is produced with machinery supplied by the company. In addition to machinery and equipment for the entire production process, Raute's service concept includes service from spare parts to maintenance and modernizations. With approximately 700 employees, Raute serves customers from ten countries while head office is located at Nastola, Finland. (Raute Oyj, 2019.)

Aim of this thesis is to study possibilities of sandwich structure and define panel element dimensions to handle defined load conditions. The desired result is to find modular panel structure that could be utilized as roof and wall element. Research questions were set as below:

- What are the main dimensions of panel core?
- Do inlets have special characteristics in sandwich structures?
- How should core and surface sheets be attached?
- How should panels be attached as continuous structure?

This thesis relies on literature, as behavior of metal sheet structures are widely researched. To make sandwich panel designing easier, this thesis compiles information for specific purpose. Previous study of global behavior of the structure was utilized to evaluate suitable design loads. Scientific part of this thesis focuses on plate and beam theory with addition of sandwich structure theory. As a result of this thesis, created Excel-based dimensioning tool was compared to Creo 4.0 FE-analysis results.

The subject was limited to certain corner of pre-defined worst case in sense of loads and dimensions, made of S355 steel. The structure is considered as statically loaded, therefore fatigue behavior is ignored. As the structure is used at elevated 300°C temperatures, gluing methods are not covered because of creep tendency. The thesis is limited to simplified seismic action behavior modelling, as it is suggested type for preliminary designing of structures. Expense and material corrosion comparison to the existing structure are ignored, as well as detailed manufacturing aspects.

2 ANALYZING OF METAL SHEET STRUCTURE

Structures may become inoperative in several ways. Instead of allowed stress analysis, Eurocode 3 dimensioning is based on limit state analysis and partial safety factors, where characteristic loads are magnified to design loads and material characteristic features are reduced to design values. (Niemi 2003, p.14.) Figure 1 illustrates the criteria of structural analysis.

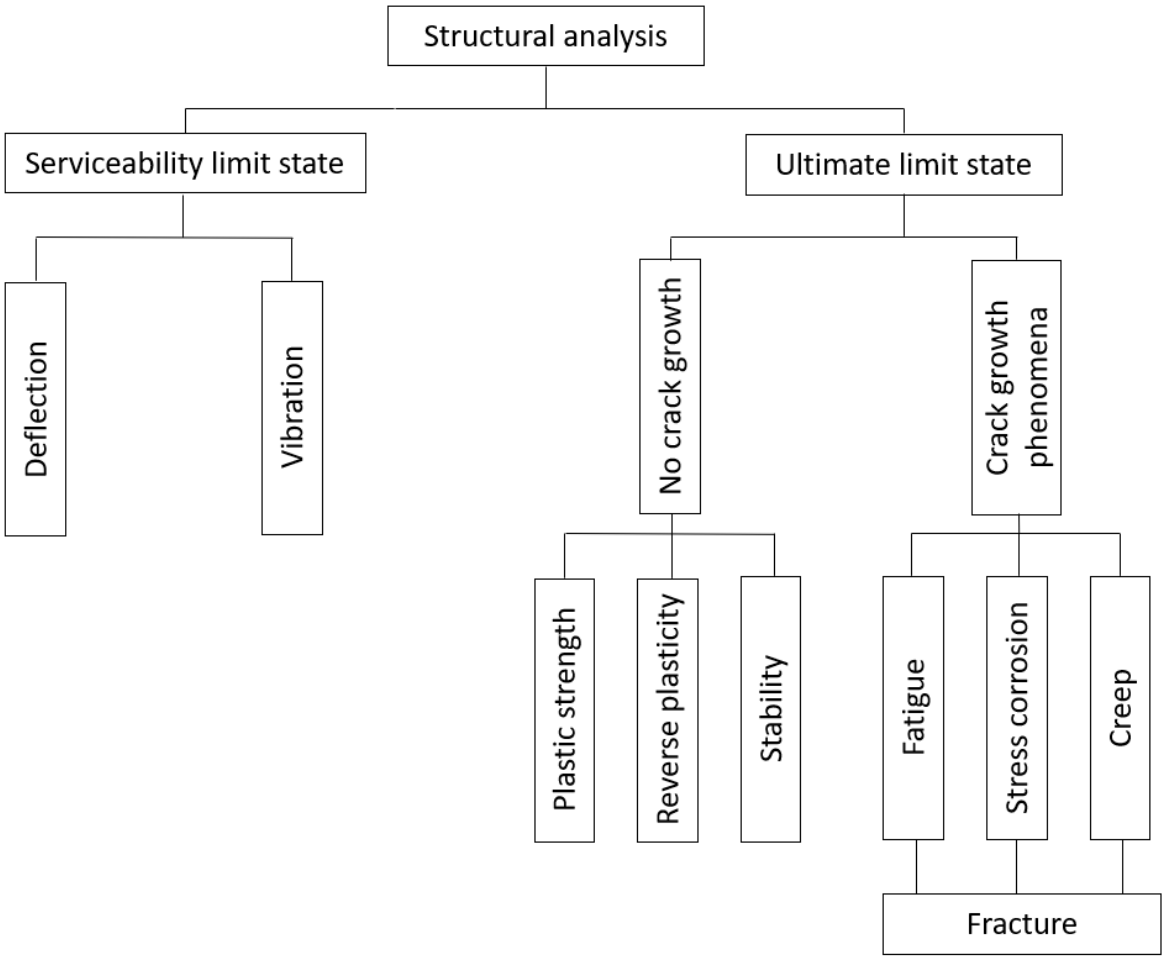

Figure 1. Structural analysis according to Eurocode 3 (Niemi 2003, p.14).

According to Davies (2001, p.231), failure modes of sandwich structures in serviceability and ultimate limit state can be divided into seven phenomena, illustrated in figure 2:

a) tensile strength of the face
b) compressive strength of the face
c) shear strength of the core

d) strength of the face and core on the support
e) strength of the connections
f) shear strength of the web
g) support reaction capacity

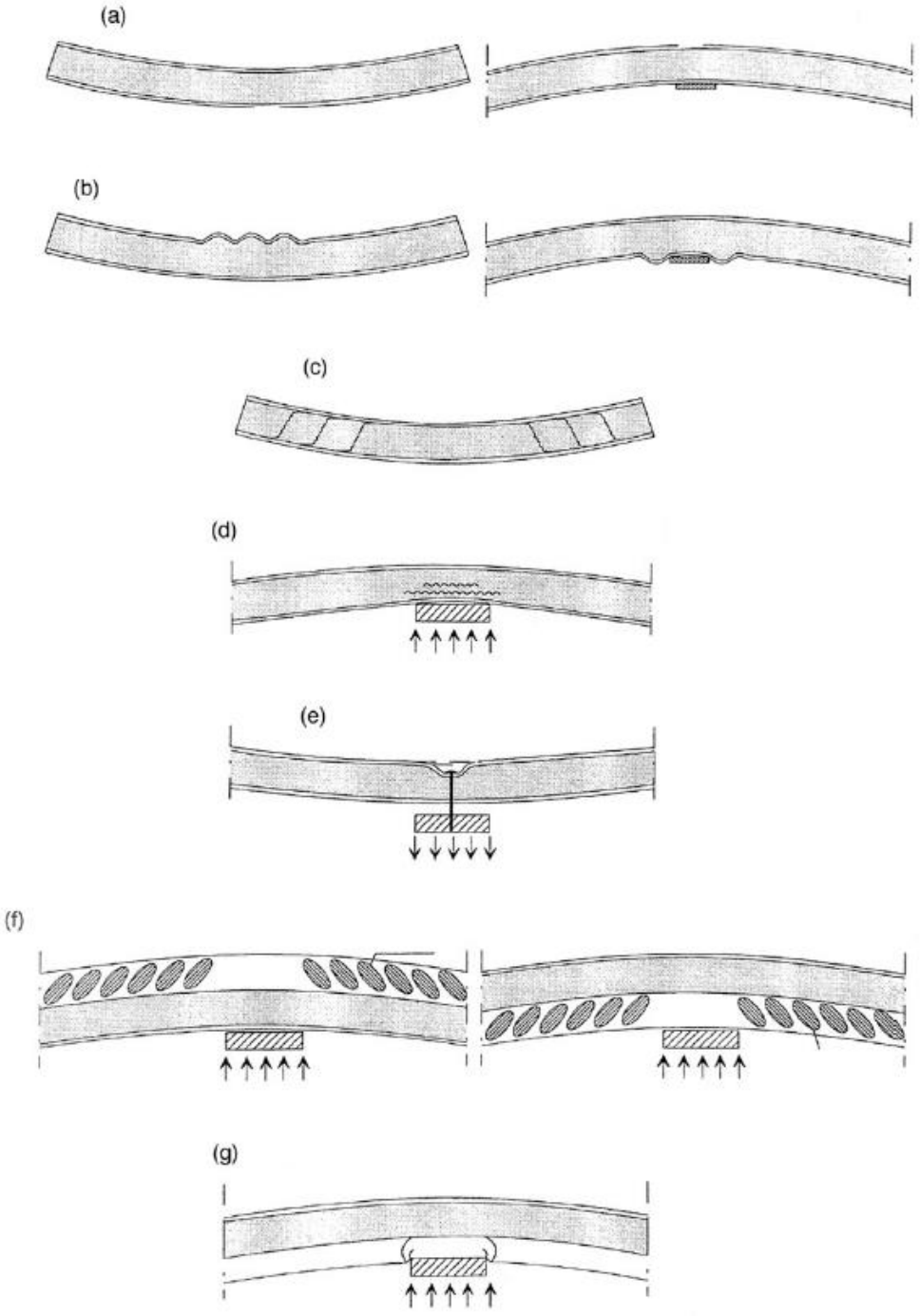

Figure 2. Failure modes of sandwich panel (Davies 2001, p.231).

Effect of elevated temperature to mechanical properties of carbon steel is described in SFS-EN-1993-1-2. Reduction factors k_θ for yield strength f_y and young's modulus E_a in propotion to 20°C temperature as illustrated in figure 3.

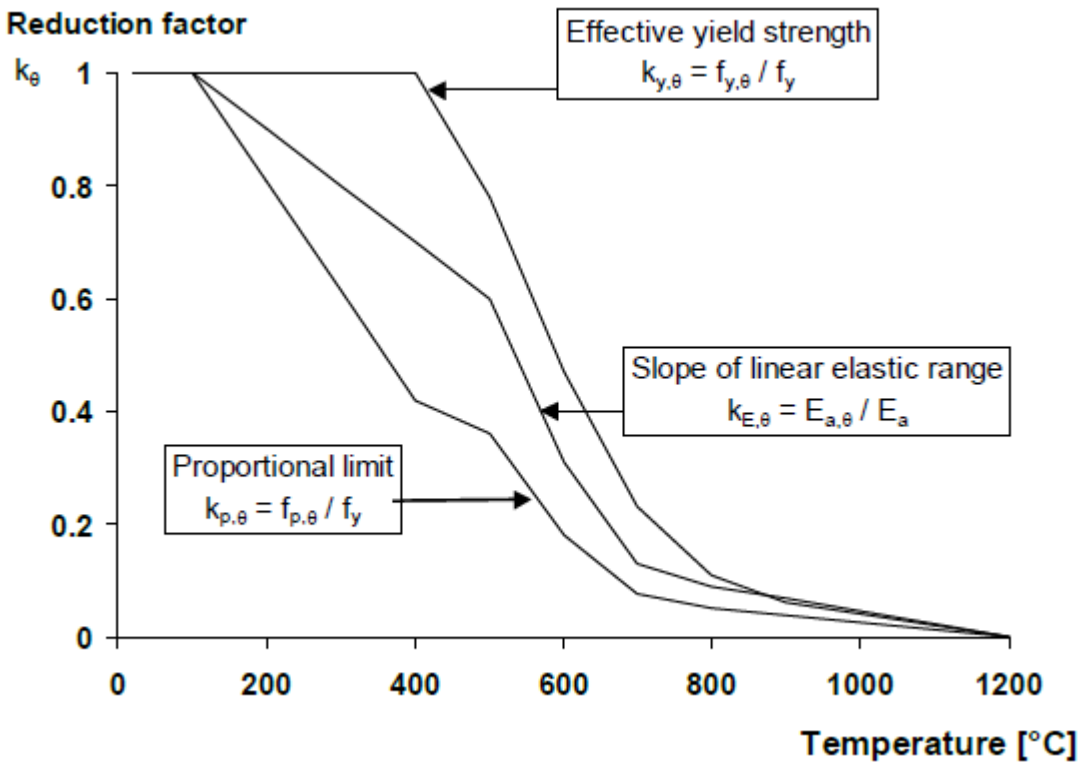

Figure 3. Reduction factors for carbon steel at elevated temperatures (SFS-EN 1993-1-2 2005, s.23).

2.1 Serviceability limit state

Serviceability limit state is a state where structure becomes inoperative (Niemi 2003, p.14). According to SFS-EN-1990 (2006, p.55), verification should be based on criteria concerning deformations that affect to the appearance, comfort of users or the functioning of the structure and vibrations that cause discomfort to people or limit the functional effectiveness of the structure.

Deflection of beam is the most common limit state and these limiting values can be found in the design guide. Serviceability limit state is analyzed only with characteristic loads without safety factors. (Niemi 2003, p.14).

2.1.1 Elastic behavior of beam

A relatively slender, long and straight object is called beam, if it is loaded with loads other than longitudinal direction. In two-dimensional level, for example xy-plane, equilibrium equations are (Pennala 2000, p.39):

$$\sum F_x = 0 \tag{1}$$

$$\sum F_y = 0 \tag{2}$$

$$\sum M_z = 0 \tag{3}$$

In two-dimensional case, single point has three degrees of freedom (=d.o.f). The point has two translational and one rotational d.o.f. Removal of d.o.f is called boundary condition.

Loaded beam forms deflection curve, illustrated in figure 4. According to Pennala (2000, pp. 91-93), when small deflection theory is assumed, and cross-section planes remain planar, correlation between deflection and cross-section properties can be derived as:

$$\frac{1}{r} = \frac{M}{E \cdot I} \tag{4}$$

where r is radius
M is the bending moment
E is Young's modulus
I is second moment of area

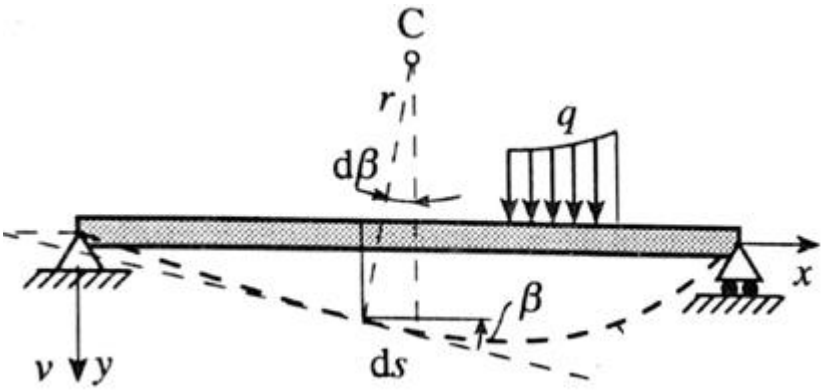

Figure 4. Deflection curve of loaded beam (Pennala 2000, p.91).

A beam is statistically over-determined (hyperstatic), if the number of equilibrium equations is lower than unknown reaction forces. In these cases, unknown reactions can be calculated using tabulated cases and compatibility conditions related to deflection curve (Pennala 2000, pp. 99 & 104).

To resist deflection, second moment of area *I* is defined. For solid rectangular hollow section, second moment of area can be defined as below (Pennala 2000, p.61):

$$I = \frac{b \cdot h^3}{12} \tag{5}$$

where *b* is width

h the height of the cross-section

Figure 5 clarifies the definition.

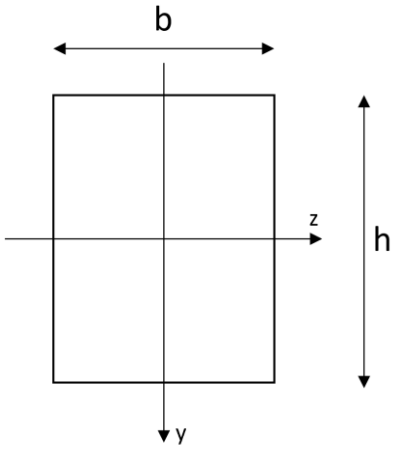

Figure 5. Definition of second moment of area *I*.

According to equation 5, increasing of height *h* increases second moment of area power three. In pure bending situation of sheet structure, normal stress distribution in symmetric beam behaves as illustrated in figure 6. In neutral axis, normal stress σ is zero. To optimize the structure, material near neutral axis should be removed and add height of the cross-section.

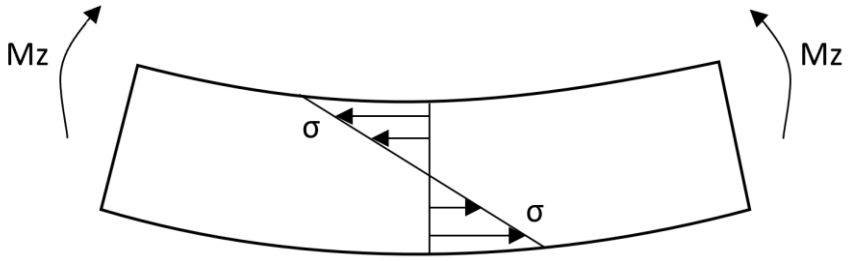

Figure 6. Normal stress distribution in pure bending.

Second moment of area for non-solid profile is defined as:

$$I = b \cdot \frac{H^3 - h^3}{12} \tag{6}$$

where optimal second moment of area can be calculated with variables defined above (Pennala 2000, p.61). Figure 7 clarifies the definition.

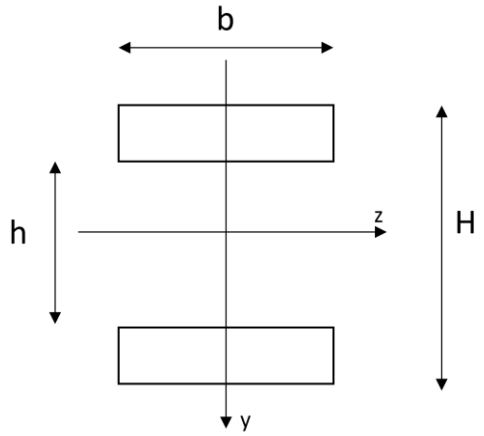

Figure 7. Definition of the *I* for non-solid profile.

Theoretically, even 80% of weight saving can be achieved with the same bending resistance when cell structure is compared to ordinary sheet structure (Kujala et al. 2003, p.3).

Common deflection limit for steel structure is *L*/300, where *L* is the span between supports (Kujala et al. 2003, p.17).

2.1.2 Vibration

Vibration is movement of physical system around equilibrium. Structures, machines and machine parts are mechanical systems in which mass and stiffness are divided. Vibrations in structures and machines are mostly harmful, appearing increased stress level, decreased lifetime and interference between machines nearby. (Pennala 1999, p.11.)

The knowledge of vibration of single degree of freedom (=d.o.f) is important, as complicated systems can usually be separated to many independent single d.o.f case (Pennala 1999, p. 31). Figure 8 illustrates some typical single d.o.f systems.

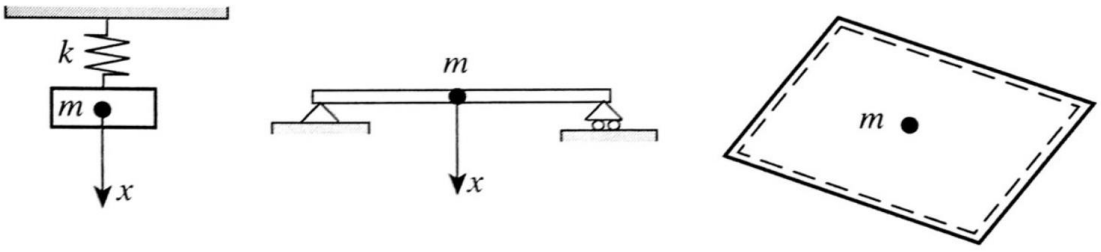

Figure 8. Some typical single d.o.f cases (Pennala 1999, p. 31).

In vibrating mechanical system, there is at least one point assumed mass *m* and spring *k*, so that system has one d.o.f. In practise, damping and impulse are related to the system. In figure 8, mass *m* moves only in direction *x*. In general case, mass *m* has six d.o.f, meaning three translational and three rotational d.o.f about coordinate axis. As continuous parametric system has infinite number of d.o.f, number of natural frequencies and vibration modes is infinite. In practise, we are interested in the lowest natural frequencies. (Pennala 1999, p. 13.)

Equation for homogenous undamped system can be written as (Pennala 1999, p.14):

$$m_1 \cdot \ddot{x} + k \cdot x = 0 \tag{7}$$

where m_1 is mass and

$\ddot{x}$ is second time derivate of displacement, acceleration

k is spring constant

x is displacement.

From equation 7, natural angular velocity ω_n can be deduced (Pennala 1999, p.37):

$$\omega_n^2 = \frac{k}{m_1} \tag{8}$$

To solve frequency based on equation 8, following equation can be used (Pennala 1999, p.22):

$$f = \frac{\omega_n}{2 \cdot \pi} \tag{9}$$

2.1.3 Earthquake

Lateral force method and response spectrum method are the most common methods in earthquake analysis. The utility of these methods is based on the fact, that earthquake behavior is statistical, and the worst loading conditions can be found with these calculations. (Kullaa, Leino & Kärnä 1998, p.14.)

Vertical shear force distribution of structure is described with lateral force method. This method is mainly used in designing of simple structures and complicated structures' pre-designing phase. The calculated force distribution is handled as static force. The computed horizontal force resembles wind force. (Kullaa et al. 1998, pp.16-17.)

As seismic loads are described with elastic response spectrum of acceleration, response spectrum method is the most common dynamic analysis method. Maximum accelerations of structure are described with function of natural period. In addition, response spectrum is also a function of relative damping. Local soil affects also to the shape of elastic design spectrum. (Kullaa et al. 1998, p.18.)

Simplified response spectrum analysis is very consistent with lateral force method, and horizontal load F_b in both main horizontal directions is described as below (Kullaa et al. 1998, p.18):

$$F_b = S_{a,d}(T) \cdot m_{tot} \tag{10}$$

where $S_{a,d}(T)$ is the design spectrum with function of natural period T
m_{tot} is the mass of the structure

Natural period T can be calculated as below (Kullaa et al. 1998, p.10):

$$T = \frac{1}{f} \tag{11}$$

According to Craig (1981, pp.503-504), the design spectrum $S_{a,d}(T)$ can be solved as an acceleration value with help of figure 9. Another option is to use peak ground acceleration (PGA) values, which can be derived from the national standard of the target country (Teräsrakenneyhdistys 2013, p.3).

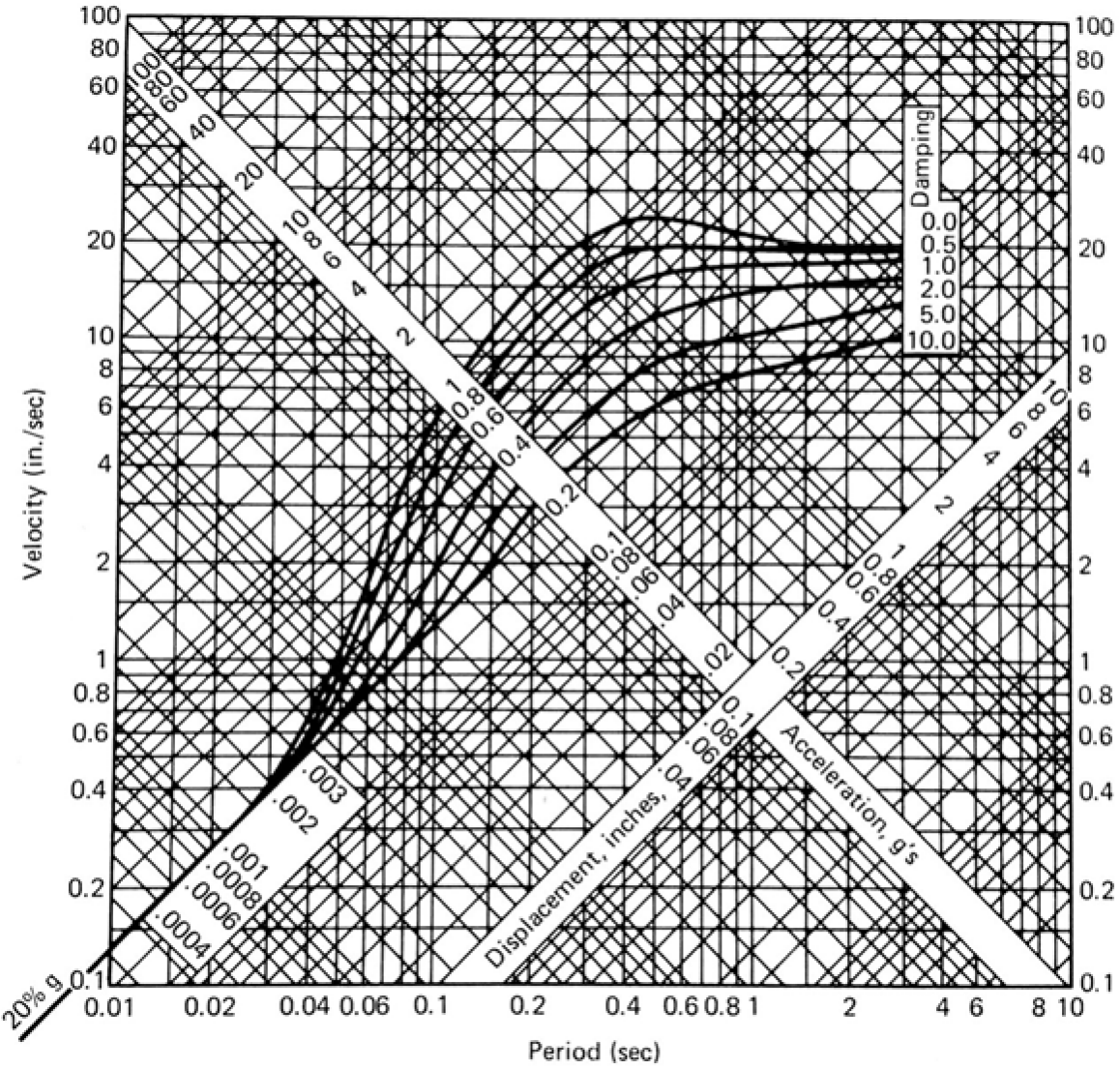

Figure 9. Tripartiate plot of design spectrum (Craig 1981, p.504).

2.2 Ultimate limit state

Ultimate limit state is related to ensuring the durability of the structure. Durability can be related to yielding or instability of the structure. In some cases, fatigue phenomenon is also related to ultimate limit state. (Niemi 2003, p.14-16.) Fatigue review is not covered by this thesis.

According to SFS-EN-1990 (2006, p.53), ultimate state limit concerns to safety of people and/or safety of the structure, and it is a state prior to structural collapse.

2.2.1 Plastic strength

The plastic limit is situation, where plastic deformation starts to grow as material yields. Only primary stresses are taken into account. (Niemi 2003, p.14.)

A simple bending case of a beam can be studied as below (Niemi 2003, p.14):

$$\gamma_F \cdot M_k \leq \frac{W \cdot f_y}{\gamma_M} \tag{12}$$

where γ_F is partial safety factor for loading
M_k is value for bending moment
W is section modulus
f_y is the yield strength of material
γ_M is the partial safety factor for material

2.2.2 Stability of a plate

Buckling is a phenomenon which must be taken into account in design phase of sheet structure. As a definition, ideal plate is a planar plate without residual stresses. This structure can be studied as grate structure illustrated in figure 10.

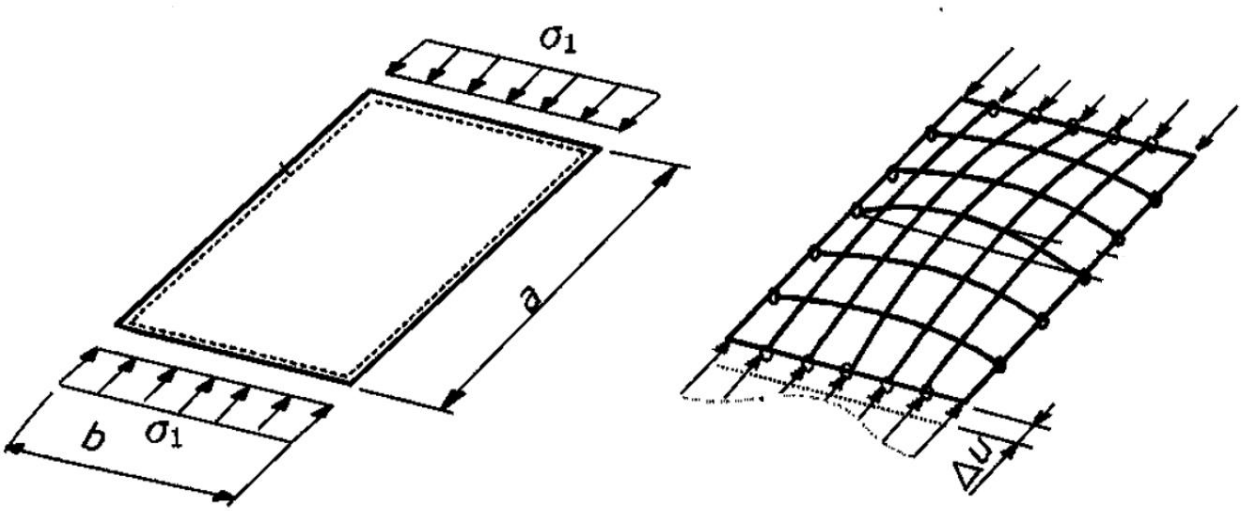

Figure 10. Ideal hinged plate under compressive stress. Buckled grate model on the right side. (Niemi 2003, p.17.)

Before critical stress level σ_{cr}, plate is elastically compressed, remaining planar. At critical stress level disruption makes plate deflect like a sine wave, because equilibrium of the plate is indifferent. Length of the plate decreases by quantity of Δu, therefore the compressive force makes external work equal to $\sigma_{cr} bt \Delta u$. (Niemi 2003, p.17.)

If plate is considered as grate structure illustrated above, it can be seen that only longitudinal beams tend to buckle. The transverse, hinged beams try to prevent the phenomena, acting like springs. As the compressed edge of buckled plate remains straight, it can be noticed, that the middle longitudinal beams are longer than those around the edges. Therefore, the compressive stress is not equally distributed, meaning that the edges are more load-bearing. The stress σ_1 means average membrane stress at the edge of plate. Only membrane stresses remain active in buckling, and local bending moment stresses can be ignored in stability analysis. (Niemi 2003, p.17.)

Instead of one longitudinal half wave, in long plates m number of half waves is born depending on relation a/b, illustrated in figure 11.

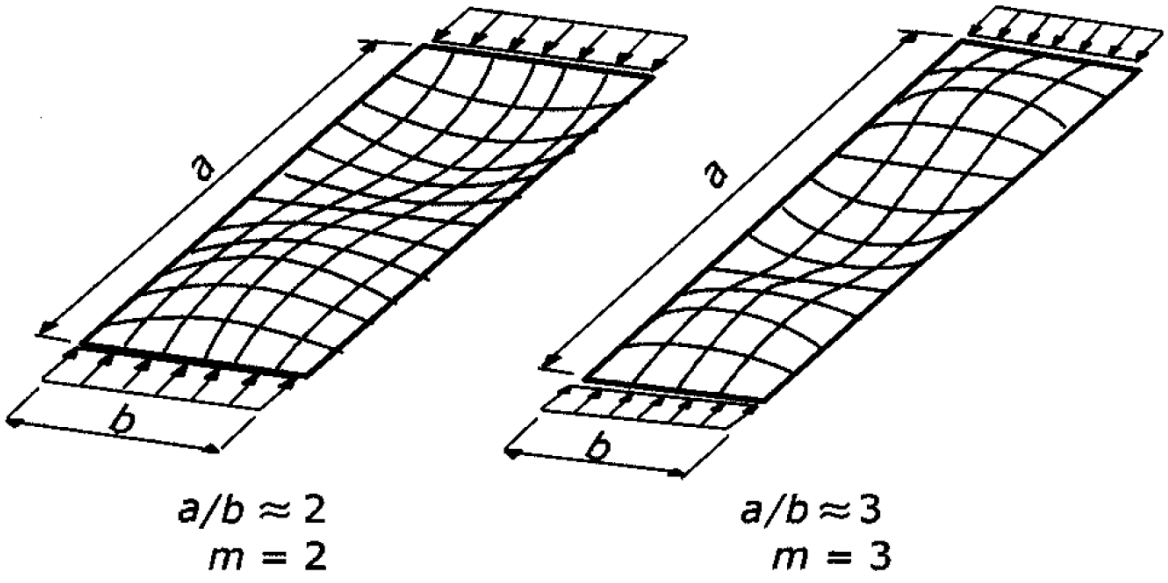

Figure 11. Buckling mode of plate with high *a/b* ratio (Niemi 2003, p.17).

Critical compressive stress σ_{cr} is defined as (Niemi 2003, p.18):

$$\sigma_{cr}=k_{\sigma}\cdot\frac{\pi^2\cdot E}{12\cdot(1-\nu^2)}\cdot\frac{t^2}{b^2} \tag{13}$$

where k_{σ} is buckling factor, depending on boundary conditions and *a/b* ratio
E is elastic modulus of material
ν is Poisson's ratio
t is thickness of plate
b is width of the plate

Simplified equation can be written as:

$$\sigma_{cr}=k_{\sigma}\cdot\sigma_{E} \tag{14}$$

where σ_e is buckling stress of the plate called Euler stress. Euler stress is always calculated the same way without taking boundary conditions into account. (Niemi 2003, p.18.)

Values for buckling factor k_{σ} are defined for example in EN 1993-1-5 for simple load and boundary conditions. The value is defined by *a/b* ratio and the number of half waves *m* in the length *a* (Niemi 2003, p.18). Figure 12 gives idea of k_{σ} definition.

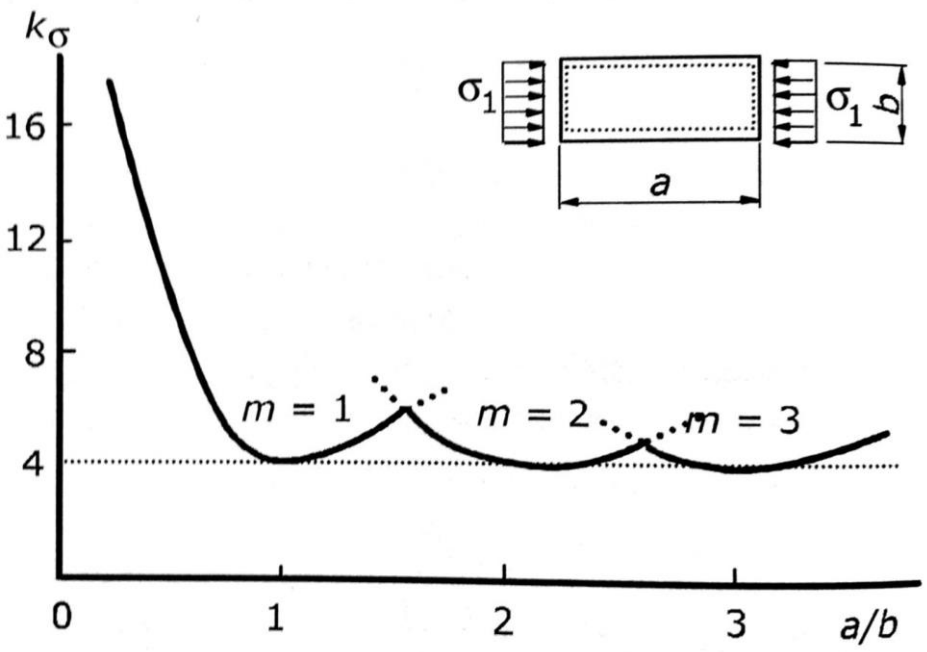

Figure 12. Definition of k_{σ} in specific load and boundary condition (Niemi 2003, p.18).

Not only the compressive stress affects buckling, but also shear stress. Pure shear stress τ is formed from two principle stresses, as illustrated in figure 13. The compressive principal stress strives to cause buckling, whereas tensile principal stress pulls the plate. As a result, antimetric buckling figure is created. (Niemi 2003, p.19.)

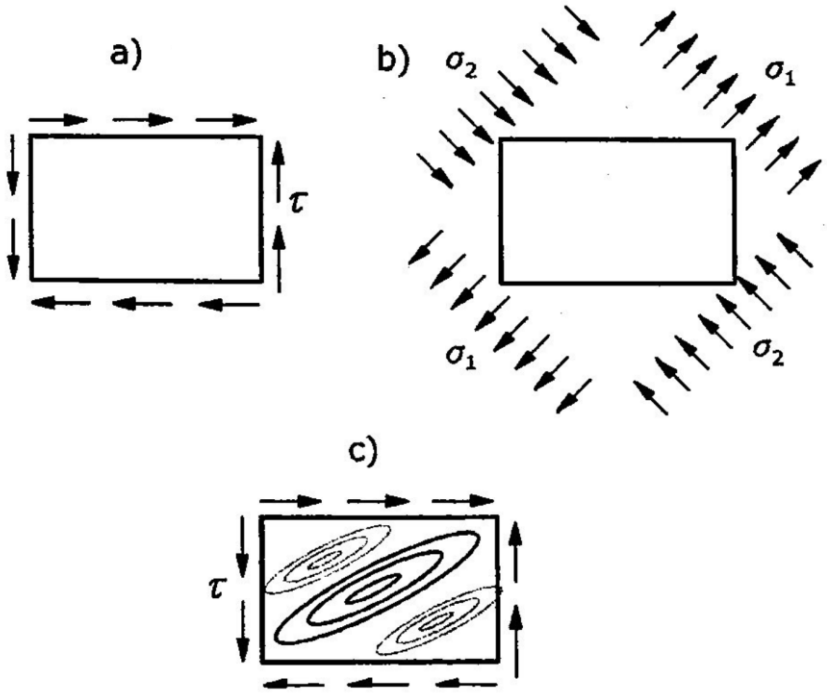

Figure 13. Shear stress divided into principal stresses, situation a) equal to b). As a result, buckling figure c). (Niemi 2003, p.19.)

According to Ongelin & Valkonen (2010, p.155), critical buckling under shear stress for unstiffened web should be checked, if

$$\frac{h_w}{t_w} > \frac{72 \cdot \varepsilon}{\eta} \tag{15}$$

where h_w is the height of the web
t_w is thickness of the web
η is the factor for strain hardening

Under 400°C for steel quality S235-S460, η = 1,2 can be used (Ongelin et al. 2010, p.153).

Variable ε in the equation 15 is the ratio of material yield strength. For elevated temperatures, it is defined as below (SFS-EN 1993-1-2 2005, p.27):

$$\varepsilon = 0{,}85 \cdot \sqrt{\frac{235}{f_y}} \tag{16}$$

2.2.3 Cross-section class 3

The purpose of cross-section classes is to define the extent of local buckling in limiting of cross-section performance. Cross-section classes are divided into four classes. The cross-section class depends on width-thickness -ratio and stress state of plate field. It is possible, that different parts of the same cross-section belong to different classes, and the class may vary depending on loading case. (Ongelin et al. 2010, p.77.)

Cross-section class 3 is described as below:
The entire cross-section is effective, as illustrated in figure 14. In bending loading case, compressive stress level may increase up to yield strength at the outermost part of the cross-section, being flange or web. The cross-section buckles before internal moment has increased up to plastic bending strength in the cross-section. In the evenly compressed cross-section, the entire section may reach yield stress level. (Ongelin et al. 2010, p.77.)

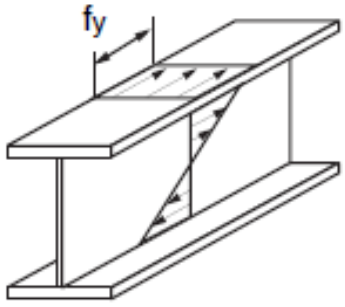

Figure 14. Cross-section class 3 principle (Ongelin et al. 2010, p.79).

According to Ongelin et al. (2010, p.120), section modulus for asymmetric cross-section can be calculated as below:

$$W_{\text{el.c}} = \frac{I}{e_{\text{c}}} \tag{17}$$

$$W_{\text{el.t}} = \frac{I}{e_t} \tag{18}$$

$$W_{\text{el}} = min[W_{\text{el.c}}\,,\, W_{\text{el.t}}] \tag{19}$$

where $W_{\text{el.c}}$ is the elastic section modulus on compression side

$W_{\text{el.t}}$ is the elastic section modulus on tension side

I is the second moment area of cross-section

e_{c} is the distance between neutral axis and outer edge of compressed flange

e_{t} is the distance between neutral axis and outer edge of tension flange

Figure 15 clarifies the calculation procedure.

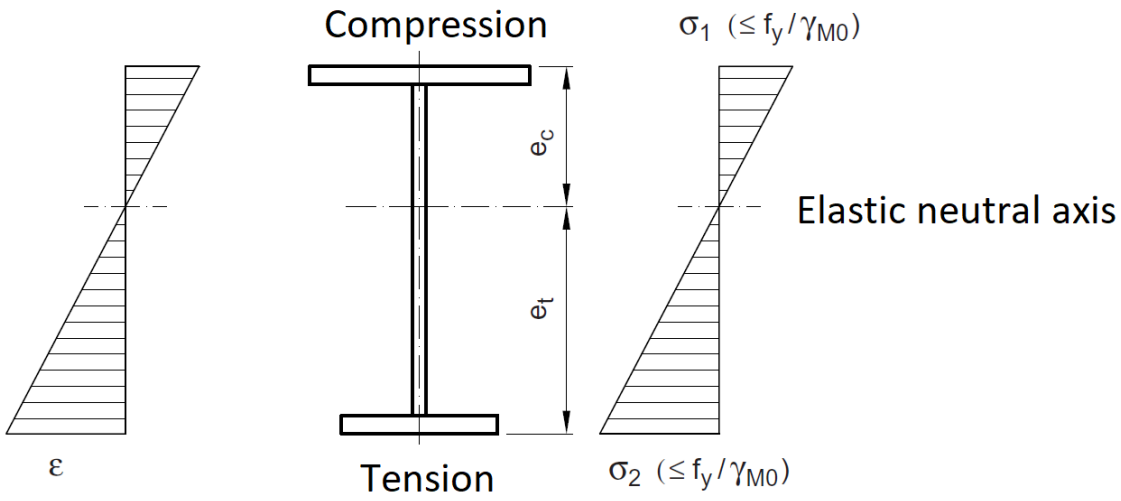

Figure 15. Stress and strain distribution of I-profile in cross-section class 3 (Ongelin et al. 2010, p.120).

According to Ongelin et al. (2010, p.120), if the structure is only loaded by bending, neutral axis location can be calculated as below:

$$z_0 = \frac{\sum A_i \cdot z_i}{\sum A_{\text{i}}} \tag{20}$$

where A_i is the area of cross-section being studied
z_i is the distance between arbitrary coordinate system and center of gravity of area A_i

When neutral axis location is known, the second moment area of cross-section can be calculated as below (Ongelin et al. 2010, p.121):

$$I = \sum \left[I_{0i} + A_i \cdot r_i^2 \right] \tag{21}$$

where I_{0i} is the second moment area of cross-section about its own center of gravity
A_i is the area of cross-section being studied
r_i is the distance between neutral axis and center of gravity of area being studied

2.2.4 Local shear resistance of unstiffened web

According to SFS-EN-1993-1-3 (2006, pp.50-51), local transverse resistance of cross-sections with two or more webs can be specified as below, if distance from support reaction or local load to free end is at least 40 mm. In addition, cross-section must satisfy following criteria:

$$\frac{r}{t} \leq 10 \tag{22}$$

$$\frac{h_w}{t} \leq 200 \cdot \sin \emptyset \tag{23}$$

$$45° \leq \emptyset \leq 90° \tag{24}$$

where h_w is the height of the web, defined by distance between flanges
r is the inner radius of the corner
$\emptyset$ is the angle between web and flange

Figure 16 clarifies the definition of web local resistance against crippling.

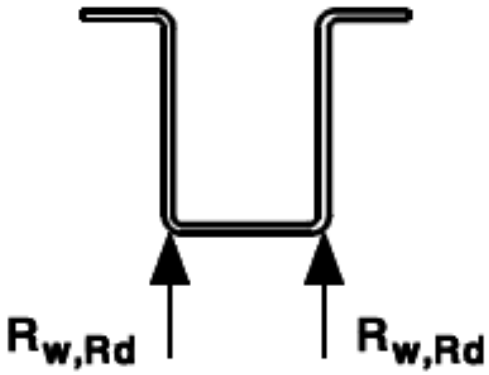

Figure 16. Local transverse resistance of web (SFS-EN-1993-1-3 2006, p.51).

Local transverse resistance $R_{w,Rd}$ for each web can be calculated as below:

$$R_{w,Rd} = \alpha \cdot t^2 \cdot \sqrt{f_y \cdot E} \cdot \left(1\text{-}0.1 \cdot \sqrt{\frac{r}{t}}\right) \cdot \left(0.5 + \sqrt{0.02 \cdot \frac{l_a}{t}}\right) \cdot \frac{\left(2.4 + \left(\frac{\emptyset}{90}\right)^2\right)}{\gamma_{M1}} \tag{25}$$

where l_a is the effective bearing length of the relevant category
α is the coefficient for the relevant category

In category 2, term l_a is defined based on term β_v as below:

$$\beta_v \leq 0.2 \rightarrow l_a = s_s \tag{26}$$

$$\beta_v = \frac{|V_{Ed,1}| - |V_{Ed,2}|}{|V_{Ed,1}| + |V_{Ed,2}|} \tag{27}$$

where V_{Ed} values are absolute values of the transverse shear forces, and $V_{ed,1} \geq V_{ed,2}$
s_s is the length of stiff bearing

For category 2 hat profiles, α = 0.115.

2.2.5 Shear lag

The planar cross-section is assumed to remain planar under bending loading. This assumption is no longer valid in very wide flange beams, due to deformations caused by shear stresses far from web of the beam. The phenomenon is called shear lag. In the areas of rapid changing shear forces, for example beam supports, shear lag is changing rapidly also. This means decreased axial strain and stress levels far from web of the beam, as illustrated in figure 17. (Niemi 2003, p.38.)

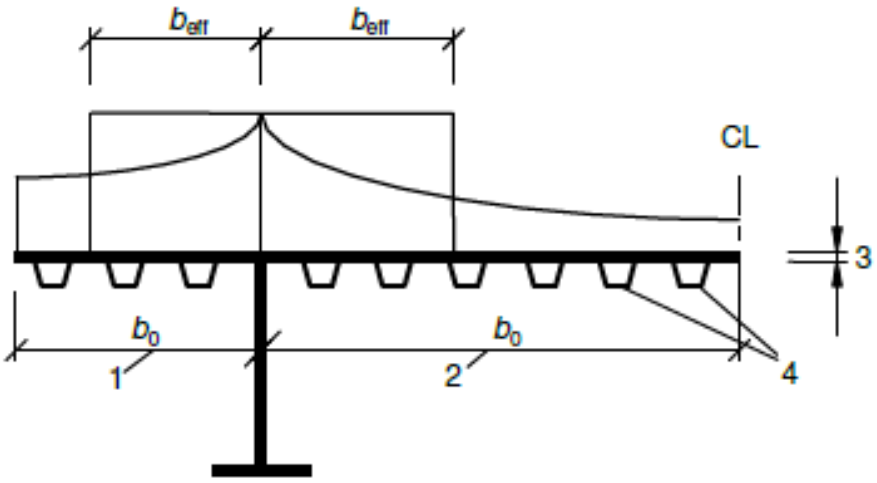

Figure 17. Principle of stress distribution and effective width formation, caused by shear lag (Niemi 2003, p.38).

According to SFS-EN-1993-1-5, shear lag in flanges can be ignored, if

$$b_0 < \frac{L_e}{50} \tag{28}$$

where b_0 is the flange outstand or half the width of internal element
L_e is the length between zero bending moment points

The effective width b_{eff} can be calculated as:

$$b_{eff} = \beta \cdot b_0 \tag{29}$$

where β is reduction factor defined in figure 18.

As β depends on parameter κ, this variable can be solved as below:

$$\kappa = \alpha_0 \cdot \frac{b_0}{L_e} \tag{30}$$

Variable α_0 can be calculated as:

$$\alpha_0 = \sqrt{1 + \frac{\sum A_{sl}}{b_0 \cdot t}} \tag{31}$$

where ΣA_{sl} is the area of longitudinal stiffeners in width b_0.

κ	Verification	β – value
$\kappa \leq 0{,}02$		$\beta = 1{,}0$
$0{,}02 < \kappa \leq 0{,}70$	sagging bending	$\beta = \beta_1 = \frac{1}{1 + 6{,}4\,\kappa^2}$
	hogging bending	$\beta = \beta_2 = \frac{1}{1 + 6{,}0\left(\kappa - \frac{1}{2500\,\kappa}\right) + 1{,}6\,\kappa^2}$
$> 0{,}70$	sagging bending	$\beta = \beta_1 = \frac{1}{5{,}9\,\kappa}$
	hogging bending	$\beta = \beta_2 = \frac{1}{8{,}6\,\kappa}$
all κ	end support	$\beta_0 = (0{,}55 + 0{,}025 / \kappa)\,\beta_1$, but $\beta_0 < \beta_1$
all κ	Cantilever	$\beta = \beta_2$ at support and at the end

Figure 18. Definition of reduction factor β (SFS-EN-1993-1-5 2006, p.10).

2.3 Finite element method

To get numerical solution for specific problem, finite element (FE) method is applicable way. FE method involves cutting structure into several elements and describing the behaviour of elements. These elements are connected together with nodes. The method is based on simultaneous algebraic equations, nodes being in equilibrium in stress analysis. Even

several thousand equations might perform in stress analysis, hence computer implementation is mandatory. (Cook 1995, p.1.)

At first stage, the FE method calculates nodal displacements and uses this information to calculate strains. Based on solution, stresses can be solved. (Cook 1995, p.7.) If a flat plate carries lateral loads, problem is called plate bending problem (Cook 1995, p.6).

2.3.1 Difference of linear and nonlinear analysis

Response to load is proportional in linear analysis. Therefore, stress is directly proportional to strain as well as load maintain the same direction when structure deforms. The assumption in this analysis type is, that displacements and rotations are small. In addition, supports do not settle. These assumptions may differ from reality. (Cook 1995, p.275.)

Various reasons, for example geometrical or material, the problem may become nonlinear. The geometrical nonlinearity can be caused by large displacements so that equilibrium equations must be written for deformed configuration. Material nonlinearity may occur due to nonlinear stress-strain relation. In addition, stiffness of the structure may be lost because of buckling of the structure. As nonlinearity makes problem more complicated, several solution steps must be taken until convergence test is satisfied. Therefore, computation time increases and results cannot be scaled in proportion to different loads. (Cook 1995, pp.275-276.)

3 DESIGN PROCEDURE OF STRUCTURE

All steel sandwich panels, where core and surface sheets are made of steel, can be divided into different categories depending on core structure: continuous corrugated and single profile stiffened sandwich structure, illustrated in figure 19 (Kujala et al. 2003, p.7).

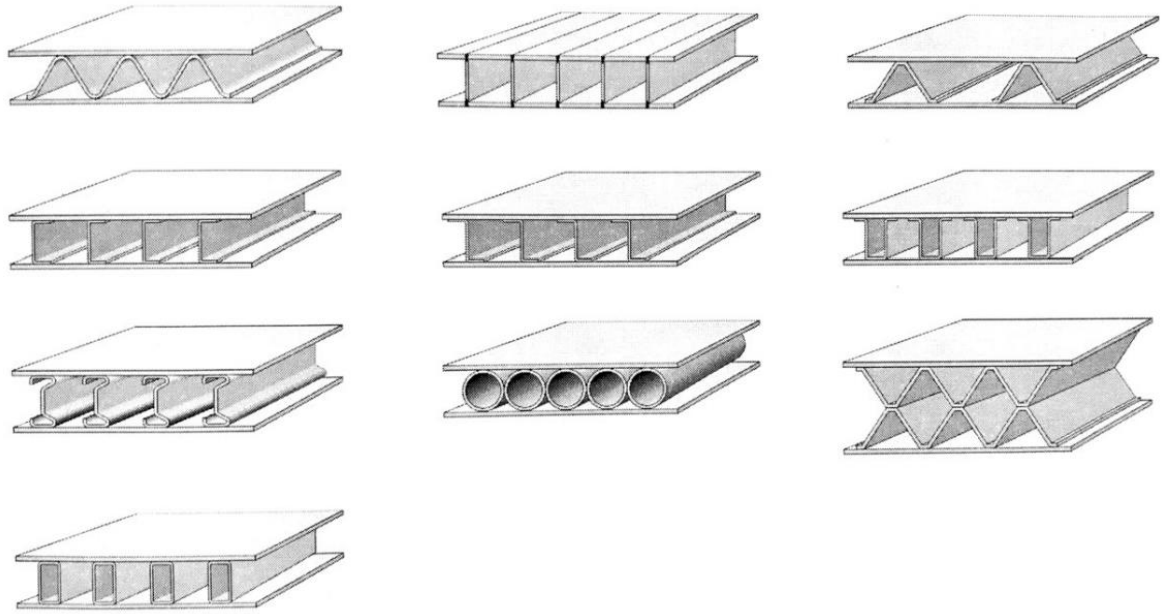

Figure 19. Different sandwich core structures (Kujala et al. 2003, p.7).

Due to efficient design of sandwich element, each component of the structure can be utilized to its ultimate limit. High stiffness-to-weight ratio and bending capacity-to-weight ratio are the most beneficial features of the structure. In addition, the absorption of mechanical energy in some deformation modes can be multiplied compared to monocoque structures, if shorter mode of buckling waves is achieved with the design. Because of low thermal conductivity of cellular cores, additional thermal insulation can be reduced. (Zenkert 1997, p.4.)

The design process of sandwich structure is illustrated in figure 20. At the beginning of design process, geometry, loads, boundary conditions and strength criteria are defined. The main principal dimensions are usually length, width and height. Depending on chosen core geometry, representing dimensions can be for example thickness of surface and core plates and angle of core plates. (Kujala et al. 2003, p.9.)

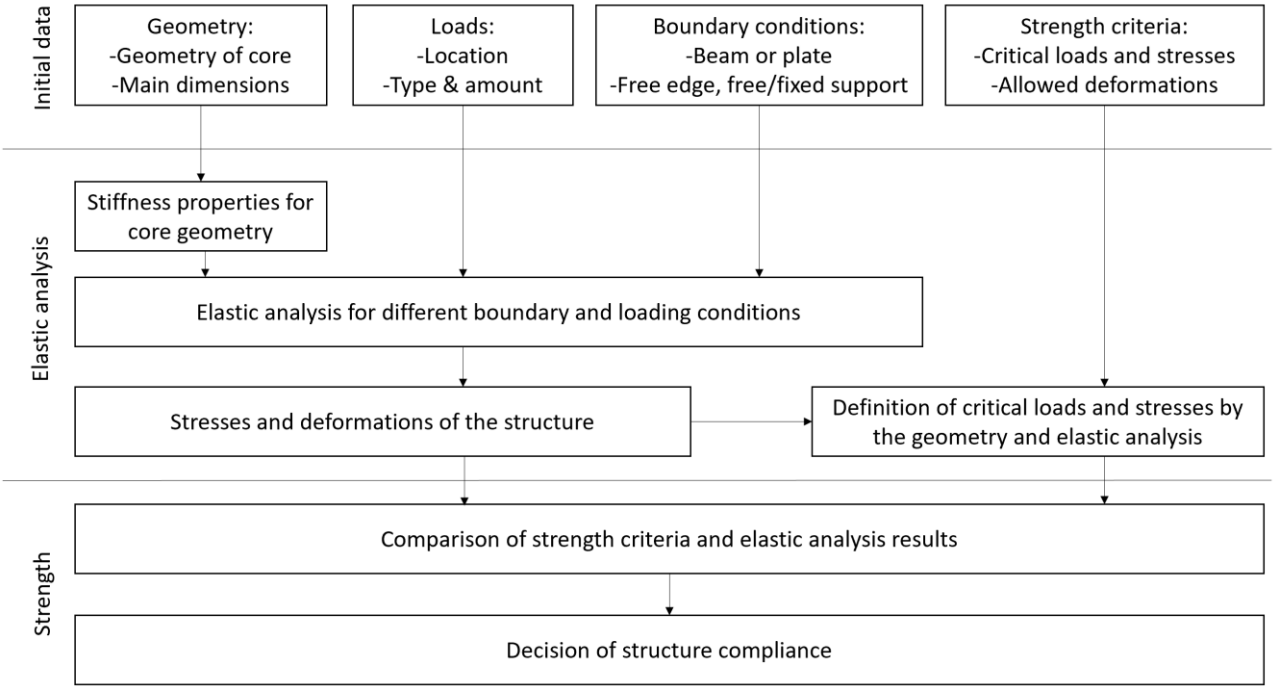

Figure 20. Design process of sandwich structure (Kujala et al. 2003, p.9).

Next stage in the design process is the definition of loads and boundary conditions. Relevant information is the location, amount and type of loading. In addition, the type of boundary condition defines the behavior of structure, being set to free edge, hinged or fixed support. Also, important definition is whether the structure behaves as plate or beam structure. Strength criteria define applicability of chosen structure depending on load and boundary condition. (Kujala et al. 2003, p.9.)

Based on initial data, definition of stiffness properties can be done. As a result of elastic analysis, deformations and stress levels can be defined. As cross-section is known, critical stress levels and forces can be defined. After this step, comparison between strength criteria and elastic analysis results can be performed. (Kujala et al. 2003, p.9.)

3.1 Optimization of cell dimensions

Metal sandwich structure can be designed in different ways depending on the accuracy and time being used. The following list compiles design methods, the first option being the most inaccurate and fastest way and the last being the most accurate and time-consuming way (Kujala et al. 2003, p.18):

- utilization of pre-calculated design graph
- utilization of beam theory and analytical calculations
- utilization of 2D plate theory and analytical calculations
- utilization of 3D FEM to solve response and use of analytical calculations
- utilization of 3D FEM to solve response and strength capacity

3.1.1 Core dimensioning

The design stress value f_{yd} can be fully utilized, if the width-thickness ratio c/t of plate field follows limit values of SFS-EN-1993-1-1. These limit values are calculated for different materials, boundary conditions, stress distributions and stress ratios. (Niemi 2003, p.22.) For internal part subjected to compression, limit value is calculated as below:

$$c/t \leq 42 \cdot \varepsilon \tag{32}$$

For internal part subjected to bending and compression, limit value is calculated as below, when $\psi \leq -1$:

$$c/t \leq 62 \cdot \varepsilon \cdot (1-\psi) \cdot \sqrt{(-\psi)} \tag{33}$$

Variable ψ in the equation 33 is the ratio of compressive and tensile stress, defined as below:

$$\psi = \frac{\sigma_2}{\sigma_1} \tag{34}$$

where σ_1 is the maximum compressive stress
σ_2 is the tensile stress

3.1.2 Face sheet dimensioning

Thickness of face sheet has significant effect on the weight of sandwich structure. Face sheet should be as thin as possible, while still having sufficient resistance against concentrated loads. One option is to calculate required sheet thickness against wheel loaded structures as below (Kujala et al. 2003, p.24):

$$t = \frac{77{,}4 \cdot \sqrt{k_w \cdot c_1 \cdot b_1 \cdot p}}{\sqrt{m_2 \cdot \sigma}} \tag{35}$$

where c_1 is height of the load [m]

b_1 is the distance between cores [m]

p is the surface pressure [kPa]

σ is the yield strength of material [kPa]

In the equation 35, k_w is calculated as below, while $k_{wmax} = 1$:

$$k_w = 1{,}3 - \frac{4{,}2}{\left(\frac{c_1}{b_1} + 1{,}8\right)^2} \tag{36}$$

In addition, variable m_2 is defined as below, when $c_1/b_1 < 1{,}0$ and $c_1 = b_1$ when $c_1 > b_1$:

$$m_2 = \frac{38}{\left(\frac{c_1}{b_1}\right)^2 - 4{,}7 \cdot \frac{c_1}{b_1} + 6{,}5} \tag{37}$$

When $c_1/b_1 > 1{,}0$, $m_2 = 13{,}57$.

Figure 21 illustrates calculated face sheet thicknesses according to equation 35 to resist different concentrated load, depending on material yield strength and distance between cores (Kujala et al. 2003, p.24).

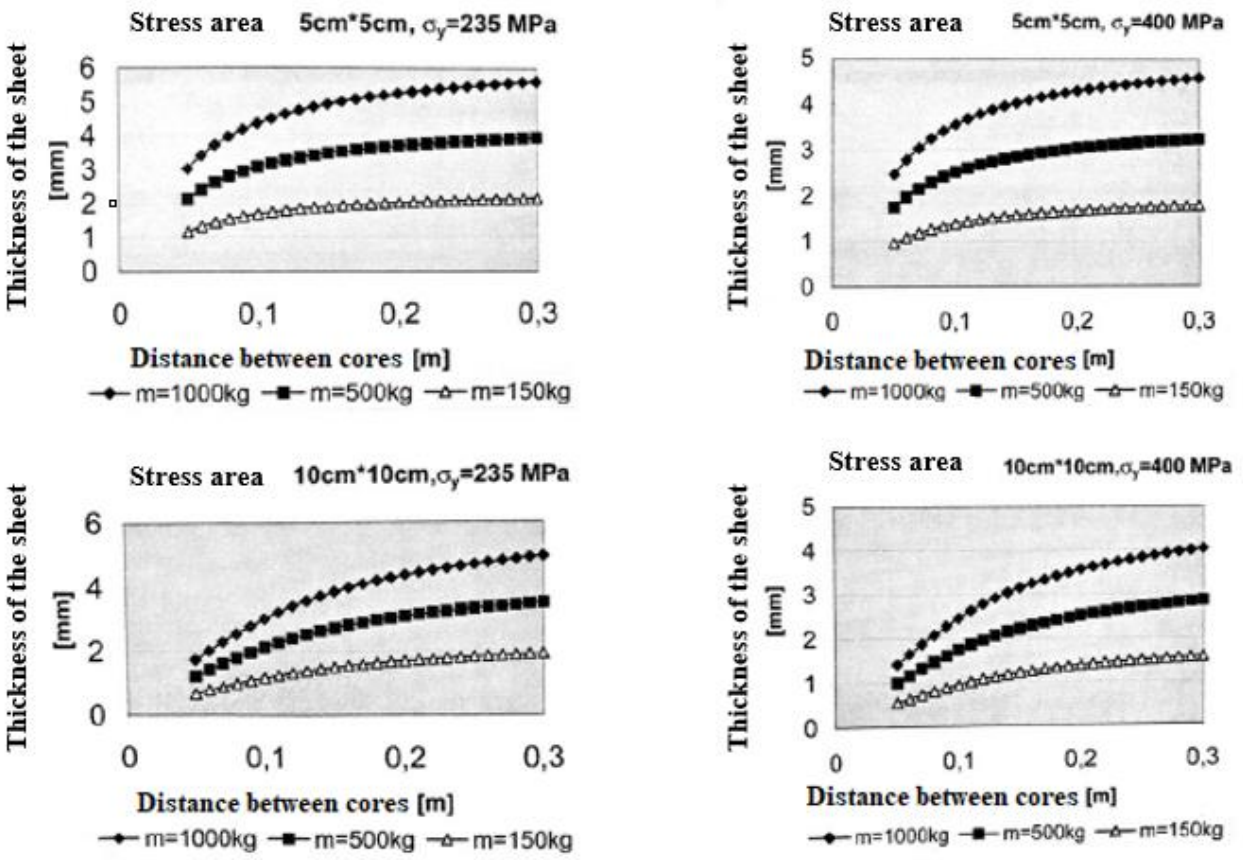

Figure 21. Required face sheet thickness for different point loads, depending on distance between cores and material yield strength (Kujala et al. 2003, p.25).

3.2 Joint between surface and core plates

Joint between surface and core plates is possible to manufacture in many ways. Depending on core structure, joint can be made by attaching core and surface plate at first stage. The second stage is to place the other surface plate and attach it. The alternative way is to attach core and surface plate and then turn the cell to attach the second surface plate. Turning may be problematic operation especially with large cells. For example, O-type cell has to be manufactured in this way. (Kujala et al. 2003, p.29.) This chapter compiles aspects of the most common ways used to join the structure.

3.2.1 Laser welding

Laser welding is an efficient welding method. Especially, welding speed becomes important when number of welds increases. This favors laser welding, as welding speed can be up to 25 m/min. (Nuutinen 1999, p.87.)

Other benefit of method is low deformation as a result of low heat input. As laser welding is piercing method, it suits well for this kind of purpose. In addition, the shape or size of manufactured cell does not limit the usage of laser welding as spot weld does. The main issue with laser welding is air gap, especially gap over 10% of sheet thickness. (Kujala et al. 2003, pp.29 & 31.)

Typical width of laser weld ligament is about 1 – 1,5 mm, hence, it is safe to assume laser attachment weld to be stronger than normal strength base material in thickness range up to 3 – 4 mm (Kujala et al. 2003, p.42). Static capacity test proved continuous laser weld to be best choice compared to spot – and intermittent laser weld (Kujala et al. 2003, p.46).

3.2.2 Spot welding

Spot welding is a potential method in sandwich structure manufacturing, if equipment is developed for large structures and core design is suitable. Low heat input and good productivity are the key features of this method. As spot welding needs support electrode, the process suits better for shorter cells. Alternative option is to use special one side spot weld process, where spot weld is made through whole structure, illustrated in figure 22. This method sets limitations for sheet thickness, as sheets must be compressed together. Also, usual limitations for spot welding are discontinuous lap joint and possibility of variable weld quality. (Kujala et al. 2003, pp.32-33.)

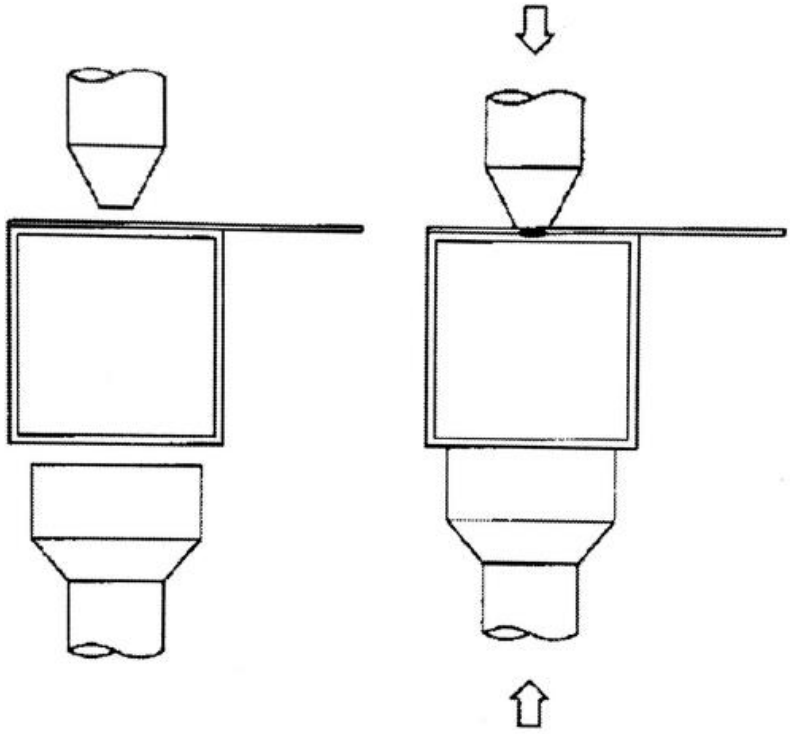

Figure 22. One sided spot welding (Kujala et al. 2003, p.33).

3.2.3 Mechanical connection

Benefits of screws and rivets are versatility and possibility to join different materials. Automated machinery has reduced expenses in series production. Self-drilling screws decrease the amount of work, while rivets need holes. The sheet thickness range with screws is usually below 2 millimeters. Benefit of mechanical connection is the lack of heat input, saving the possible coating of a sheet. The downsides of screw joint are high stress peaks and tightening torque dependent reliability. (Nuutinen 1999, pp.29-32.)

3.3 Joint between cells

Depending on loading case, joints must be able to bear shear, bending and tensile loads. Fatigue strength of the structure is defined by the weakest joint. In this respect, overlapping joint applications should be avoided. Typical edge profiles are RHS beams and C-profiles with minimum thickness of 2 millimeters, attached with traditional welding methods. Other options are casted joint pieces or bended core and surface sheets. (Kujala et al. 2003, pp.25-26.) Figures 23 and 24 illustrate these possible options.

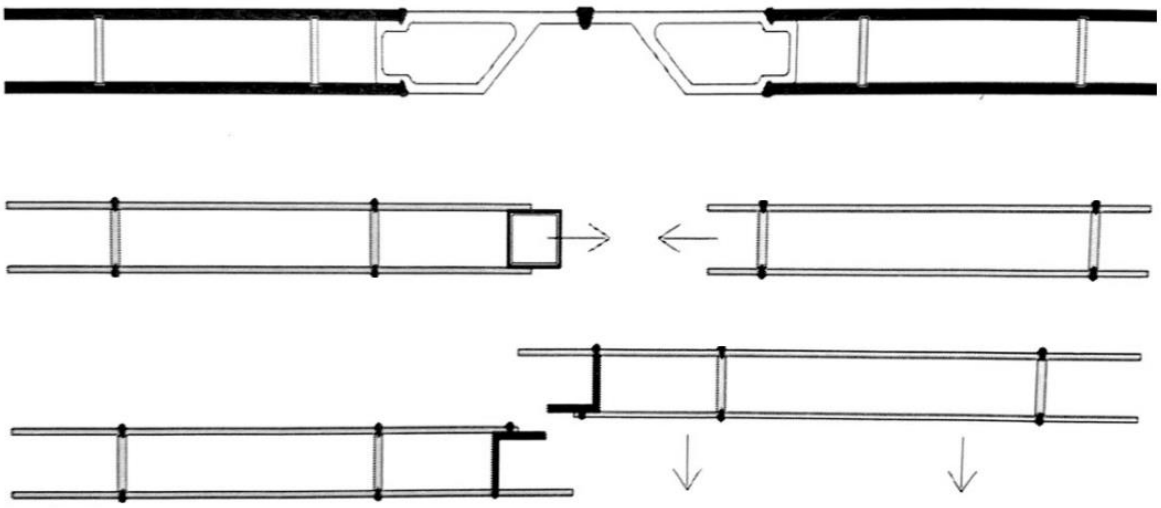

Figure 23. Common joints used between panels (Kujala et al. 2003, p.26).

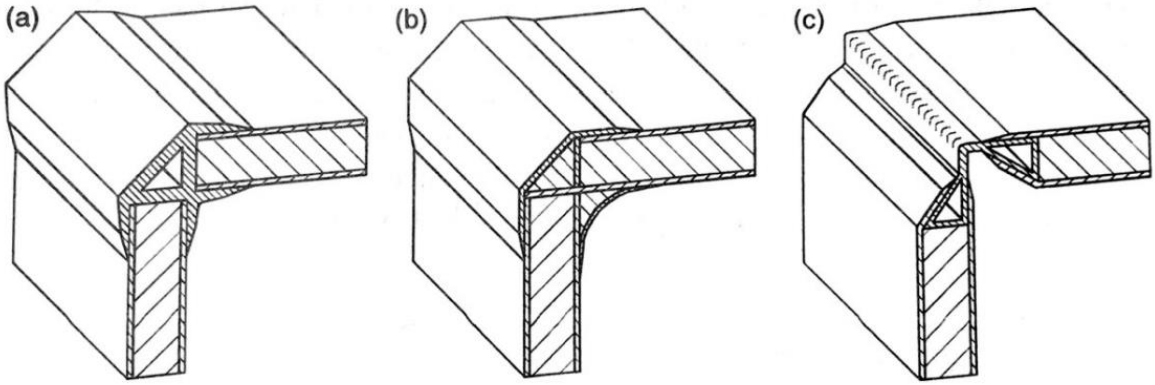

Figure 24. Possible joints used between panels (Zenkert 1997, p.236).

3.4 Throat thickness of fillet weld

Fillet weld design for arc-welded lap welds, for material thicknesses under 4 mm is instructed in SFS EN 1993-1-3. According to SFS EN 1993-1-3 (2006, p.68), with throat thickness at least equal to the thickness of connected sheet should provide sufficient resistance of the connection.

Design resistance $F_{w,Rd}$ for side fillet of a pair of side fillets is determined as below, if $L_{w,s} > b$ (SFS EN 1993-1-3 2006, p.68):

$$F_{w,Rd} = 0{,}45 \cdot t \cdot b \cdot \frac{f_u}{\gamma_{M2}} \tag{38}$$

For an end fillet, design resistance is determined as below (SFS EN 1993-1-3 2006, p.68):

$$F_{w,Rd} = t \cdot L_{w,e} \cdot \left(1\text{-}0{,}3 \cdot \frac{L_{w,e}}{b}\right) \cdot \frac{f_u}{\gamma_{M2}} \tag{39}$$

where b is the width of connected part or sheet

f_u is the ultimate strength of material

$L_{w,e}$ is the effective length of the end fillet weld

$L_{w,s}$ is the effective length of a side fillet weld

γ_{M2} of 1,25 is recommended

Figure 25 illustrates the definitions of welded detail.

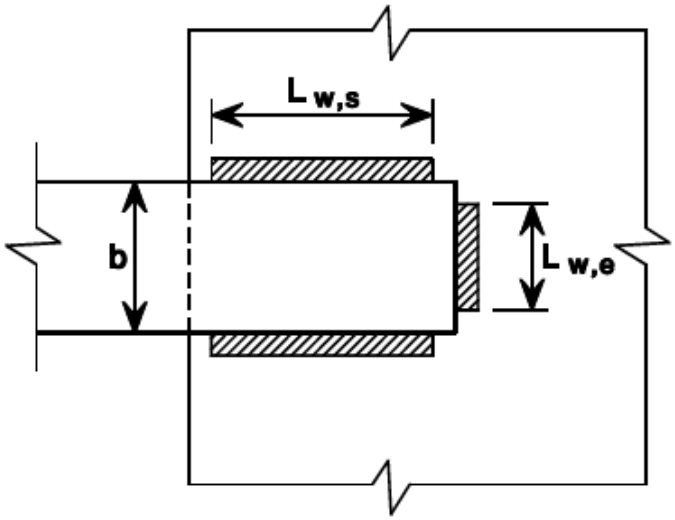

Figure 25. Fillet welded lap connection (SFS EN 1993-1-3 2006, p.69).

3.5 Effect of inlets

Inlets are typically made for piping or cabling. Sandwich structure is reinforced at the hole edge area. If the location of inlet isn't known beforehand, reinforced holes can be made in the potential areas and covered with simple plate. In the installation phase, these necessary inlets can be drilled for the desired places. (Kujala et al. 2003, p.26.)

4 PRELIMINARY DIMENSIONING OF THE STRUCTURE

The V-type core geometry was chosen based on the possibility to join core to both face sheets without turning the structure upside down. Other benefit of the V-type geometry was good lateral stiffness. The required main dimensions for the sandwich structure were: length of 6772 mm and width of 2250 mm. Hence, laser welding was chosen to be the most suitable joining method in sense of productivity.

4.1 Loads and constraints

The roof load F was simplified as single force across the width of the roof element, as illustrated in figure 26. The shear force and moment figure evaluation for this hyperstatic structure was made by dividing the roof element into two beams and assuming both corners as fixed support, illustrated in figure 27. This assumption was made, as structure is intended to be continuous at the corner, transmitting bending moment across the corner joint. The pinned support at distance of L_1 from left side is assumed to bear only shear forces.

These beams were evaluated separately with tabulated cases with guidance of Pennala (2000, pp.109-110) and Jotuni P., Ryti H. & Pöyhönen O. (1975, pp.53&54) and combined with yield line. The main load type affecting to the roof element was bending and shear loading, illustrated in figures 28 and 29.

Seismic action was evaluated with lateral acceleration of $0.4g$ in the FE-analysis. Table 1 compiles the initial data and table 2 the shear forces and bending moments. Detailed calculations can be found in appendix I.

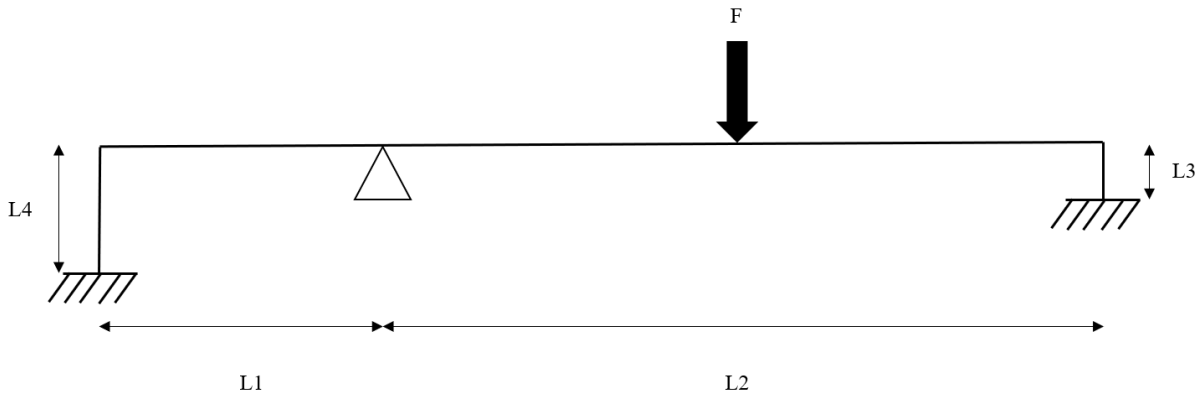

Figure 26. Load and dimensions of the roof.

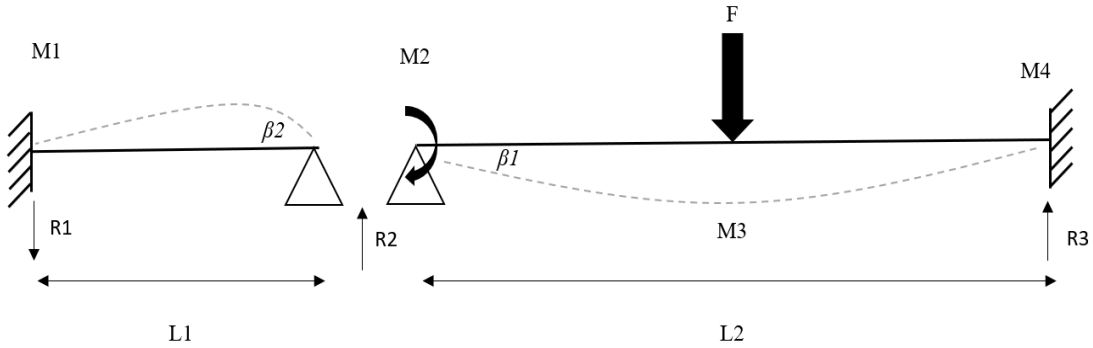

Figure 27. Hyperstatic beam divided into two beams.

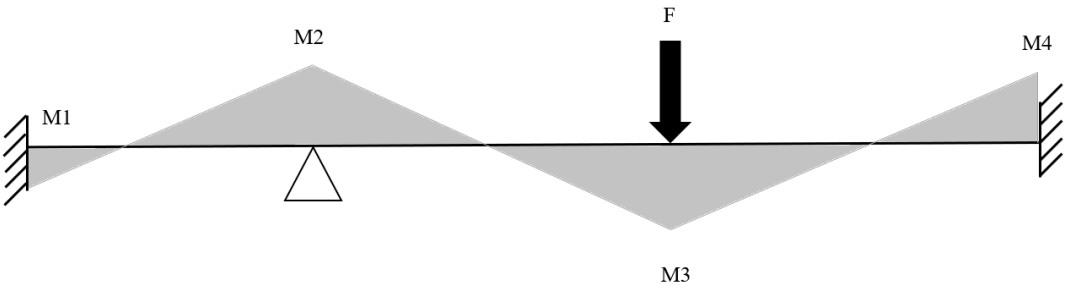

Figure 28. Moment figure of the roof element.

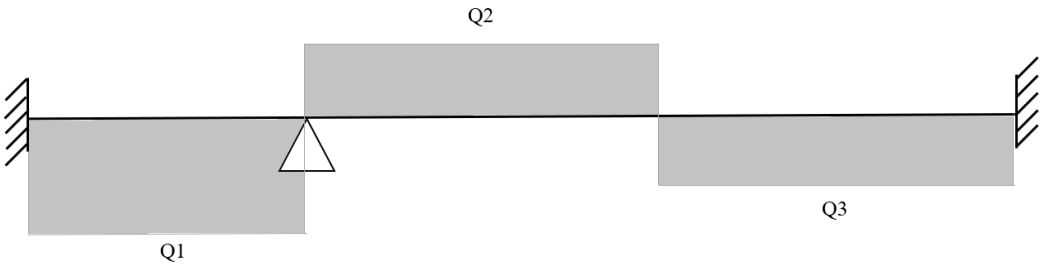

Figure 29. Shear force figure of the roof element.

Table 1. Initial data of the structure.

L_1 [mm]	1 250
L_2 [mm]	5 520
L_3 [mm]	480
L_4 [mm]	2 310
F [N]	12 825
a_s [m/s^2]	0.4*9.81

Table 2. Calculated bending moments and shear forces of the structure.

M_1 [Nmm]	-3.61*10^6	Q_1 [N]	-8 660
M_2 [Nmm]	7.22*10^6	Q_2 [N]	6 340
M_3 [Nmm]	-9.26*10^6	Q_3 [N]	-6 400
M_4 [Nmm]	9.67*10^6		

4.2 Sandwich panel

Dimensioning of the sandwich panel was based on beam theory and cross-section class 3 sheet slenderness ratios. To solve preliminary dimensions for cross-section, Excel VBA solver was created. Detailed information of the solver can be found on appendix II.

Required second moment area of cross-section was defined with section modulus and deflection limit $L/300$. With support span of L_2, allowed deflection was set to 18,4 mm. Required section modulus was calculated with equation 12 using maximum bending moment of M_4, multiplied with partial safety factor 1,5 and partial material factor 1,1. This multiplication was then divided with material yield strength.

Deflection evaluation was performed with equations below, according Pennala (2000, pp.109-110) and Jotuni et al. (1975, pp. 53&54), by using force F and bending moment M_2, length and second moment area of cross-section, illustrated in figures 30 and 31. Young's modulus at elevated 300°C temperature was reduced by 20% to value of 168 000 MPa. Deflection of the loading cases were superposed to the point C in figure 30, even though the maximum deflections will be in slightly different locations. According to Jotuni et al. (1975, pp.53&54), the maximum deflection caused by force locates with these boundary conditions

in place 0,4472*l whereas the maximum deflection caused by bending moment locates in place 0,33*l.

$$v_c = \frac{7 \cdot F \cdot l^3}{768 \cdot E \cdot I} \tag{40}$$

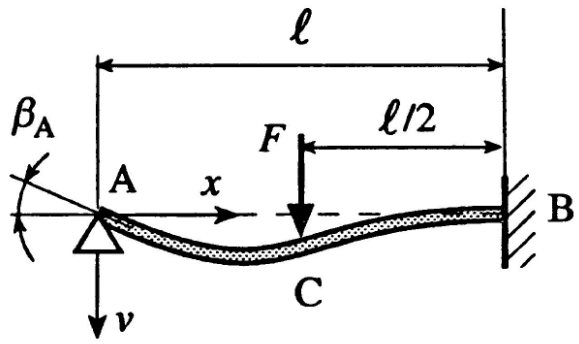

Figure 30. Deflection evaluation of beam section (Pennala 2000, p.109).

$$y = \frac{M_a \cdot l^2 \cdot \xi \cdot (1-\xi)^2}{4 \cdot E \cdot I} \tag{41}$$

In equation 41, ξ is defined as:

$$\xi = \frac{x}{l} \tag{42}$$

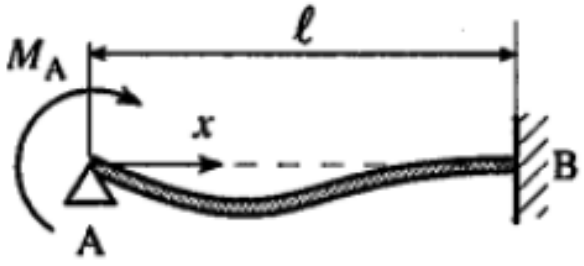

Figure 31. Deflection of the beam based on bending moment (Pennala 2000, p.110).

To calculate second moment area of cross-section, the sandwich panel was divided into *B* width and *H* height of sections, illustrated in figure 32. Number of these sections was set to the solver as integer, in range of 1-12.

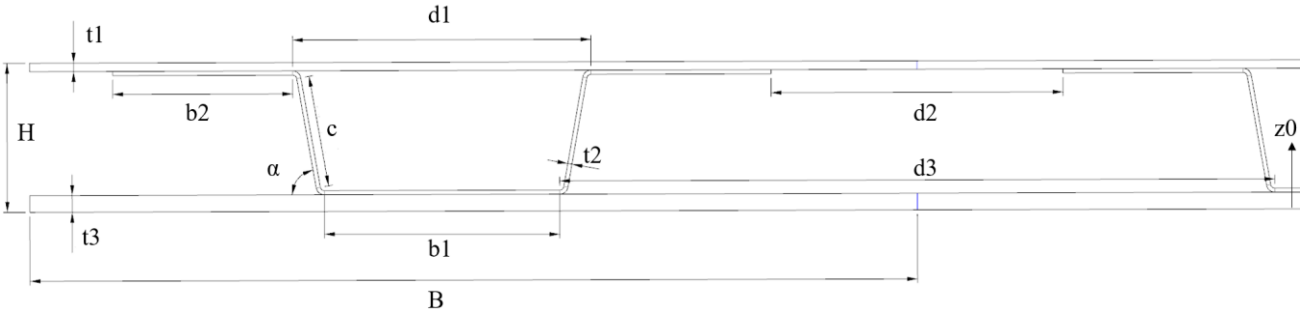

Figure 32. Variables for preliminary dimensioning.

The first calculation is related to the neutral axis location, as the cross-section remains asymmetric. The calculation is made with equation 20, using values *t*, *H*, *B*, *b*, *c* and *α*. Calculation of each plate field center of mass is started at point z_0, illustrated in the right corner of figure 32.

As the neutral axis of the asymmetric cross-section does not locate in the middle of height *H*, the second calculation was related to calculation of eccentricity related to upper face sheet. This was performed simply by reducing the neutral axis location of total height *H*.

The solver had freedom to change angle between core web and flange. Hence, center mass of core web was calculated separately from point z_0 by using values of t_2, t_3 and *α*. Also, second moment area of the web was calculated in both directions x and y. These values were used, as second moment area in y direction was calculated.

Second moment of area of tilted web was calculated based on sheet section values of *c*, *t* and angle *α* as below (Jotuni et al. 1975, p.58):

$$I_k = \frac{b \cdot h}{12} \cdot \left(h^2 \cdot cos\,\alpha^2 + b^2 \cdot sin\,\alpha^2\right) \tag{43}$$

Values of equation 43 are illustrated in figure 33. Total calculation of core second moment of area was performed using values *b*, *c*, *t*, neutral axis location and mass center point of web.

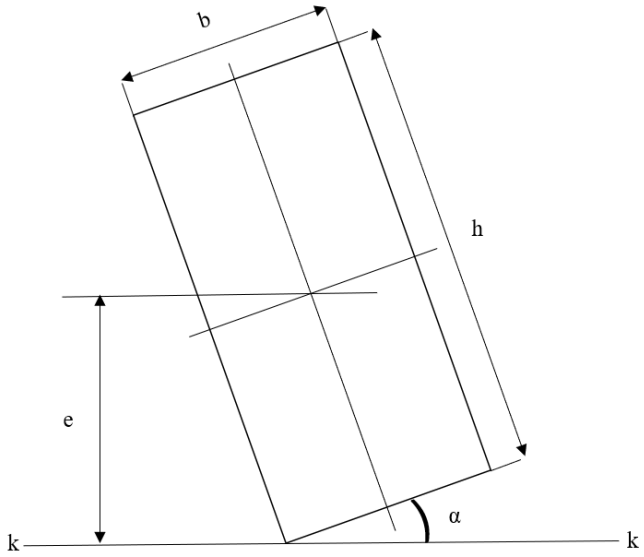

Figure 33. Second moment of area calculation around k-axis (Jotuni et al. 1975, p.58).

The total calculation of second moment of area was performed by summing up core and face sheets. Second moment of area calculation of face sheets was based on *B, t* and neutral axis location. By utilizing equations 17-19, the minimum section modulus of the cross-section was calculated and then compared to the required section modulus. Additionally, the total second moment of area was used to define deflection.

Limitations for Excel VBA solver were set by cross-section class 3 and user-defined range for values *B*, *b*, *H*, *t*, α and number of cores. For cross-section class 3, limit value for flanges was evaluated with yield strength of 355 MPa with equation 32. For the web, the limit value was evaluated with same yield strength and stress ratio $\psi = -1$, with the equation 33. Table 3 compiles the width/thickness -ratios used for different plate fields, web and flanges. Location of laser welds weren't taken into account in the plate field evaluation. This has effect to the plate field widths of d_1, d_2 and d_3.

Table 3. Limiting slenderness values for plate fields.

Stress distribution	Limit value for c/t
 flange	29
 web	85,7

With these limit values, VBA solver followed these maximum slenderness ratios in sections *c* and *d*. To avoid irrational solutions, for example sheet thicknesses were limited between range 1 – 4 mm. Also, values b_1 and b_2 were limited into range of 20 – 50 or 80 mm to enable laser weldability with additional press wheel. Also, wide flange of core sections enables larger tolerances for laser conveyor track in long panel.

All these calculations were performed by changing values of *B, b, H, t, α* and number of cores. The solver was set to minimize area of cross-section, with limitations set above. With these aspects, preliminary dimensioning was performed. Table 4 compiles the results of preliminary dimensioning of sandwich panel, with 12 cores. Deflection limit was governing the final dimensioning of cross-section. With these results, core edge pressure capacity, shear lag effect and buckling under shear stress were evaluated. Detailed information can be found on appendix III – V.

Table 4. Dimensions of the sandwich panel cross-section.

b_1 [mm]	68	d_3 [mm]	116,2
b_2 [mm]	48,3	H [mm]	45
B [mm]	184,2	t_1 [mm]	2,8
c [mm]	37,8	t_2 [mm]	1
d_1 [mm]	81,1	t_3 [mm]	4
d_2 [mm]	19,5	α [°]	80
I [mm^4]	71,8*10^5	W [mm^3]	289 124
Deflection [mm]	10,6		

4.3 Corner joint

As the main function of corner joints is to bear bending moment, preliminary dimensioning was done using beam assumption and shear load was ignored. The desired shape of the joint was angle profile, illustrated in figure 34. This solution could be attached both sides of the sandwich panel. Angle profile was idealized as fixed support beam. Based on calculated bending moment, desired length of 100 mm and deflection of 1 mm, required height of the cross-section was calculated as below, according to Pennala (2000, p.106) as illustrated in figure 35. Table 5 compiles the results of calculation.

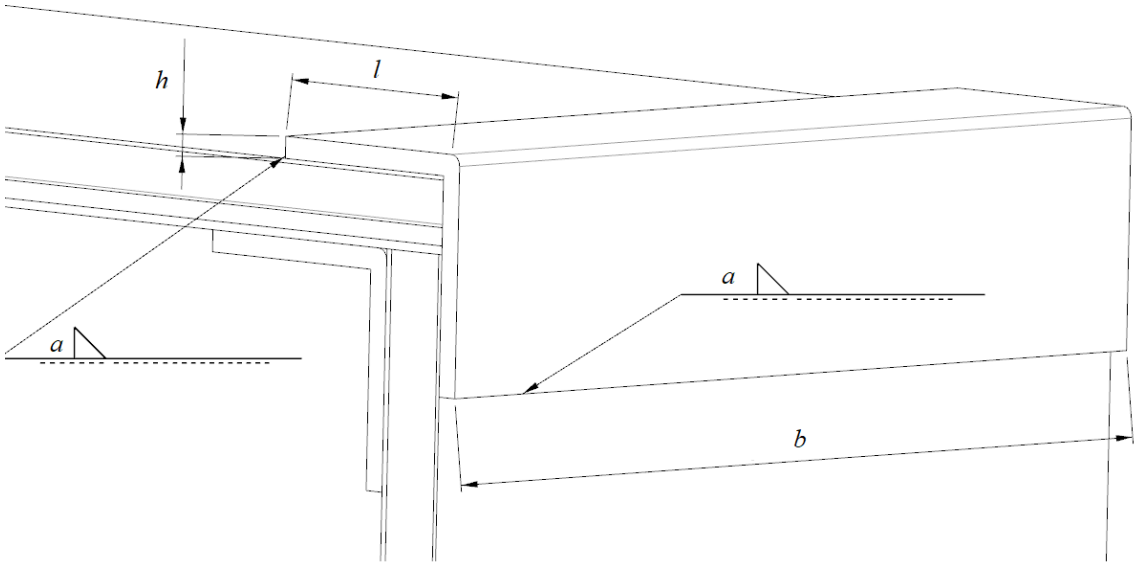

Figure 34. Dimensions of the angle profile.

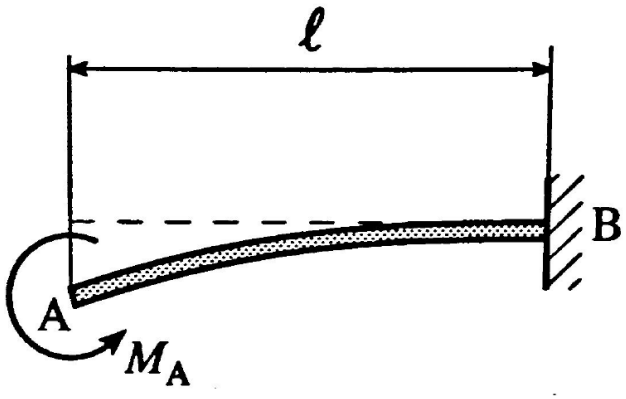

Figure 35. Idealized section of angle profile (Pennala 2000, p.106).

$$v_{max} = \frac{M \cdot l^2}{2 \cdot E \cdot I} \tag{44}$$

Table 5. Results of the corner joint calculation.

M	$9.67*10^6$ Nmm
l	100 mm
b	2 250 mm
h	11.5 mm

The attachment of the angle iron to the sandwich panel was evaluated with weld, length of whole sandwich panel width of 2250 mm. Weld throat thickness a = 3 mm for each angle profile was evaluated to be sufficient, illustrated in figure 34. In this calculation, shear lag effect was utilized to define the maximum load for fillet weld. Detailed calculations of corner joint dimensioning can be found on appendix VI.

4.4 Joint between panels

The joint between panels was treated as primary load carrying joint and secondary attachment joint in preliminary dimensioning. Only shear strength capacity was evaluated in hand calculation. The joint was designed to follow the same idea as in figure 36, therefore 40x40x3 mm RHS pipe was evaluated.

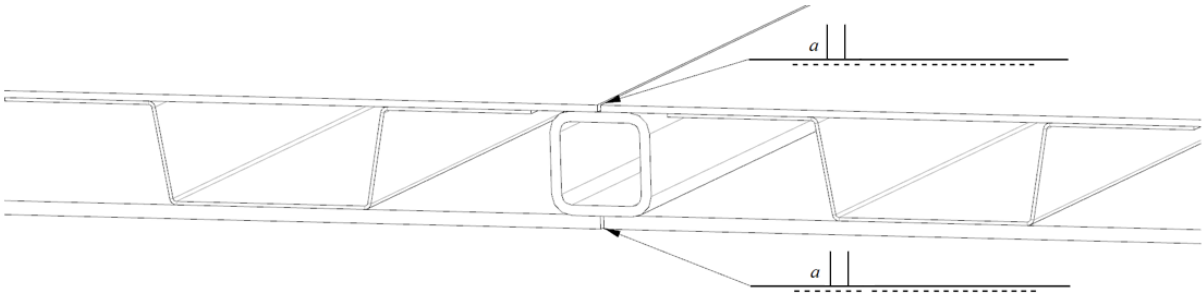

Figure 36. Chosen joint between sandwich panels.

Due to eccentricity of the load F from the center of mass, the additional torsion affects at the joint. When the welded joint is idealised as illustrated in figure 37, where the white triangles illustrate boundary condition, calculation by hand becomes challenging. Hence, effect of torsion is evaluated with FE method in chapter 5.2.

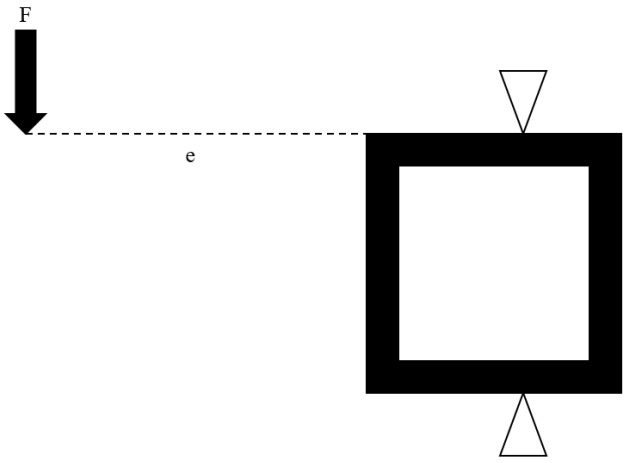

Figure 37. Load and boundary condition of idealized joint between panels.

The RHS pipe shear capacity was evaluated as below, according to Ongelin & Valkonen (2016, p.103-104):

$$V_{\mathrm{pl.Rd}} = A_{\mathrm{v}} \cdot \frac{\frac{f_{\mathrm{y}}}{\sqrt{3}}}{\gamma_{\mathrm{m0}}} \tag{45}$$

where shear area A_{v} is calculated as:

$$A_{\mathrm{v}} = A \cdot \frac{h}{b+h} \tag{46}$$

Figure 38 clarifies the definition of *h* and *b* against shear force.

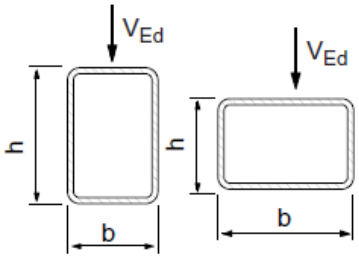

Figure 38. Definition of cross-section dimensions for shear area calculation (Ongelin et al. 2016, p.104).

The chosen joint has sufficient capacity, if it is welded with throat thickness a = t. Detailed calculations can be found on appendix VII.

5 FE MODEL AND RESULTS OF THE STRUCTURE

Sandwich panel core was modelled with bending radius equal to sheet thickness. Face sheets were assembled as sandwich structure, illustrated in figure 39. Sheet thicknesses in the model were: t_1 = 3 mm, t_2 = 1 mm and t_3 = 4 mm, slightly different from preliminary dimensioning.

The first simulation model was created with midsurface shell elements to avoid long computation time. The core was joined to face sheets with bonded interface, created with surface region, illustrated in figure 40. Element size in the first model was relatively high, 75 mm. Load and constraints were set on surface regions also, illustrated in figure 41. Unlike in analytical equations, the force was divided into two sections, to better describe the true situation. This definition leads to slightly different moment diagram and difference between analytical and simulation results, but still describing the load condition with sufficient accuracy.

Figure 39. One sixth of the sandwich structure.

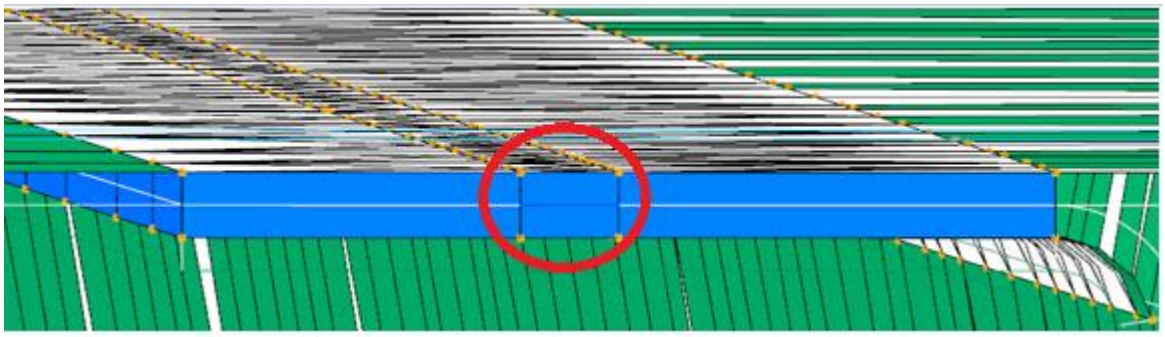

Figure 40. Bonded interface connecting face and core sheets.

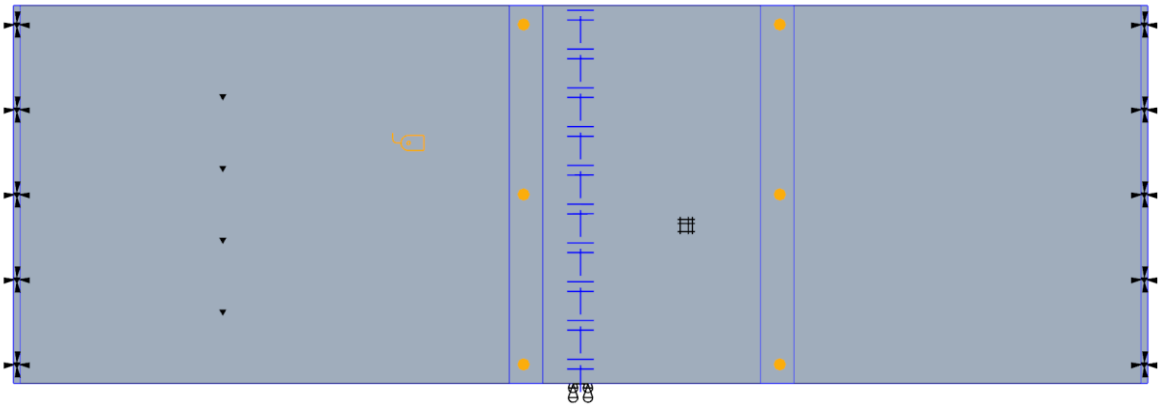

Figure 41. Forces and constraints of the structure.

One sixth of the model was also created, to reduce the simulation time. For one sixth of the sandwich panel, one sixth of the loading was used with assumption of even distribution of the stresses. Deflection comparison between full and partial model correlated with each other, hence partial model was used to study the structure. The partial model deviated from the previous, as sheets were joined with spot welds. These spot welds were modelled as beam elements between midsurfaces, as illustrated in figure 42.

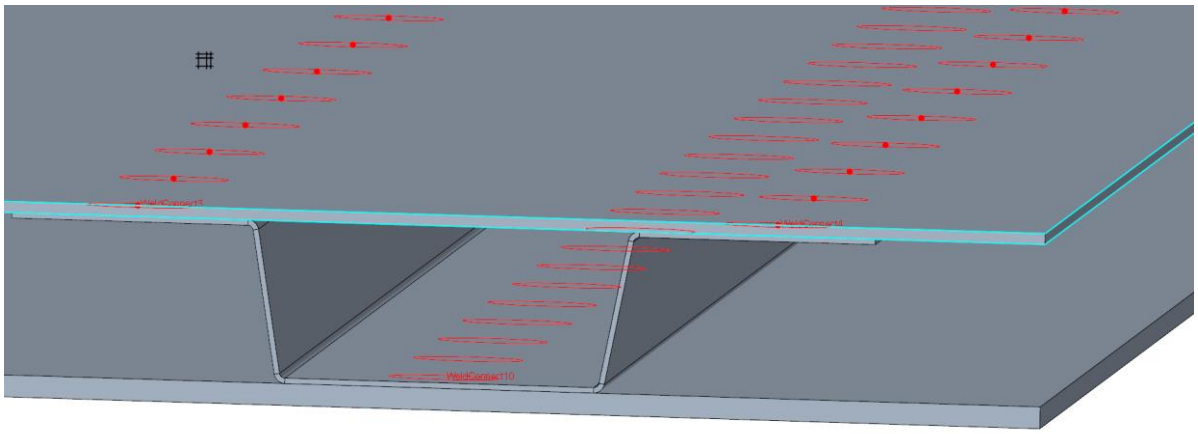

Figure 42. Beam element between face and core sheet midsurfaces.

Another simulation for partial model was performed with solid elements. Solid element was requirement to use the large displacement non-linear analysis in Creo 4.0. As non-linear analysis produced similar deflections and stress levels with linear analysis, the rest of the analyses were performed with linear analysis.

Figures 43 – 45 compile the results of FE model. Deflection is 8,8 mm, and highest von Mises stress peak, about 110 MPa, is located near corner joint marked in figure 44. Maximum von Mises stress levels of the core are illustrated in figure 45, at location of red line in figure 44. Additional buckling analysis was not performed, as face sheets do not reach yield strength of material, that is allowed in cross-section class 3. Von Mises stress levels in figures below are scaled from 0 to 200 MPa, unless otherwise stated.

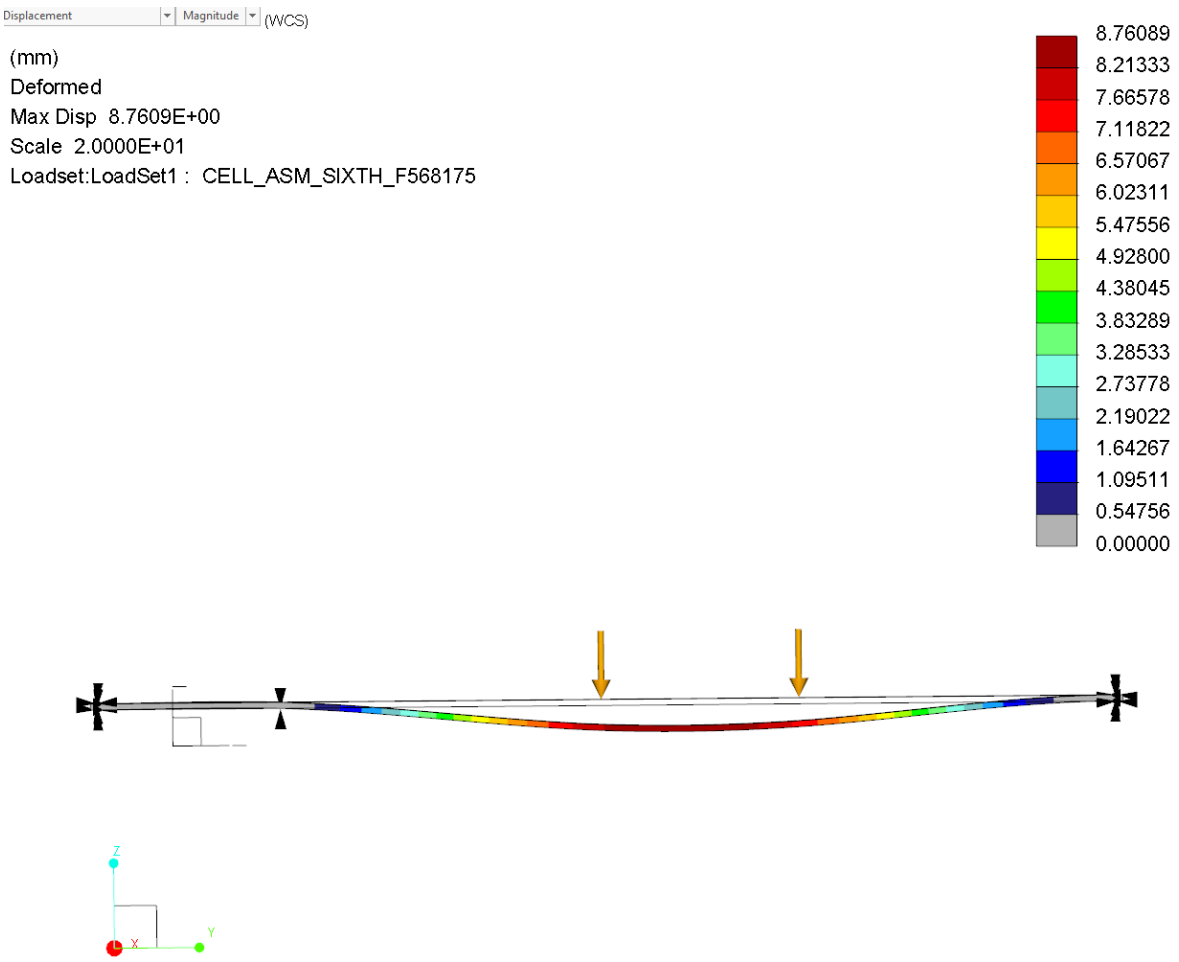

Figure 43. Deflection of the sandwich panel, scaled 20 times.

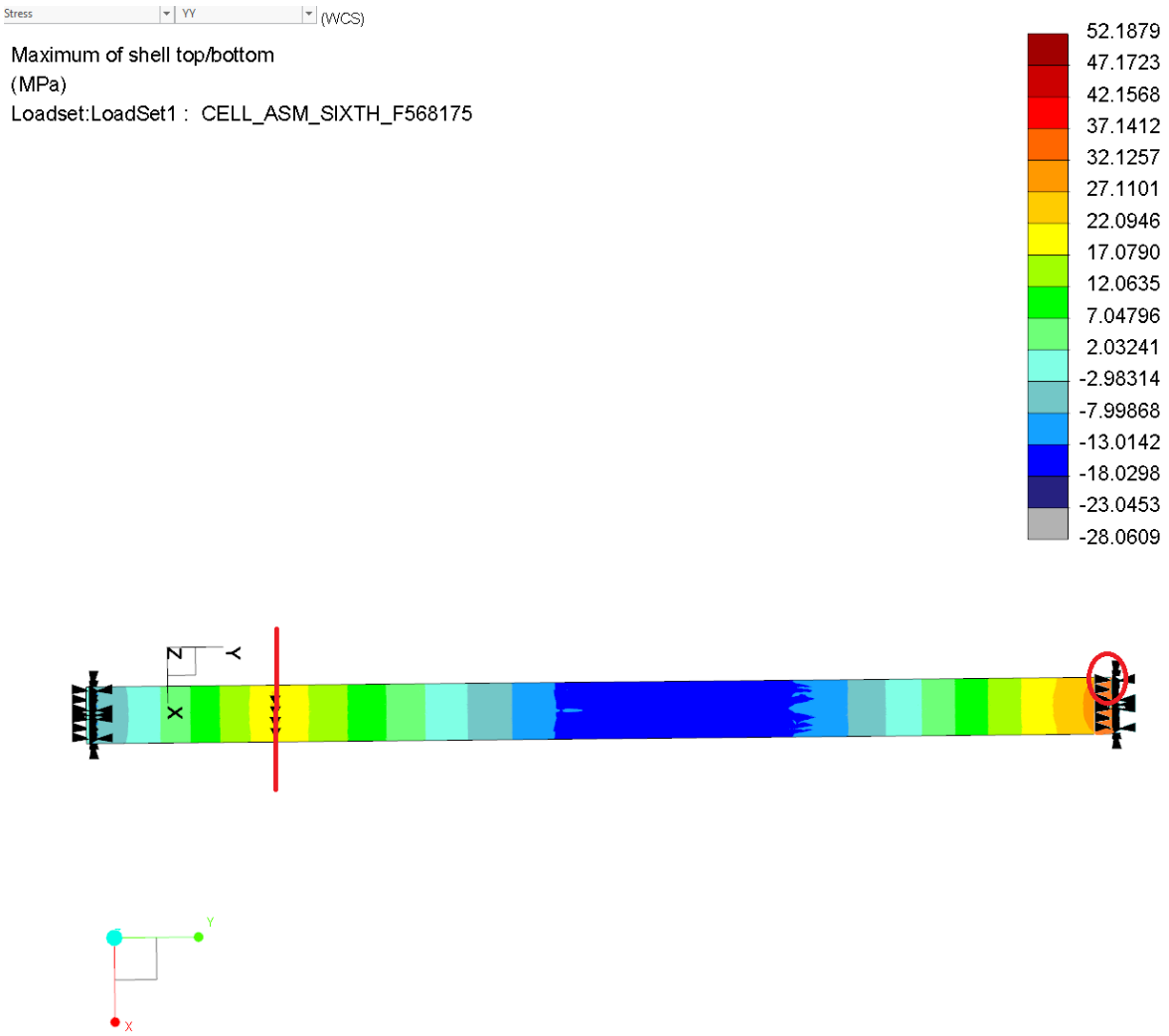

Figure 44. Nominal stress levels of face sheet.

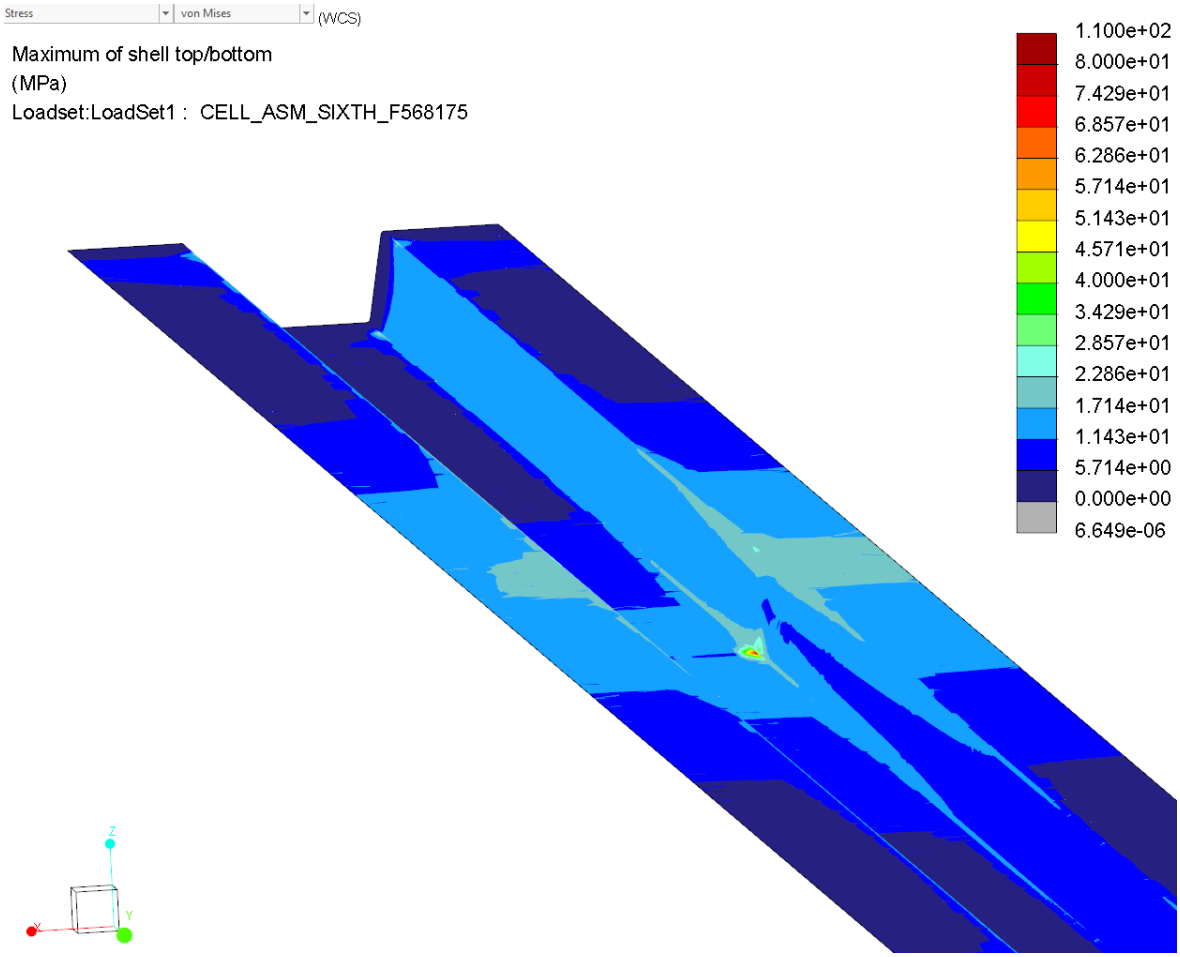

Figure 45. Maximum von Mises stress level in the core, scaled from 0 to 80 MPa.

5.1 Corner joint

The corner joint was modelled to study the stiffness based on analytical methods. Two angle profiles, with thickness of 11 mm, were assembled. In the simulation model, these angle profiles were fillet welded at each edge of angle iron and face sheet of the sandwich, as illustrated in figure 46. The weld in the simulation model was implemented as 3 mm thick element between solid element angle profile and midsurface shell element as illustrated in figure 47.

Figures 48 and 49 illustrate the results of FE model. The deflection was 1 mm and von Mises stress levels in the angle profile 25 MPa and near the weld 70 MPa.

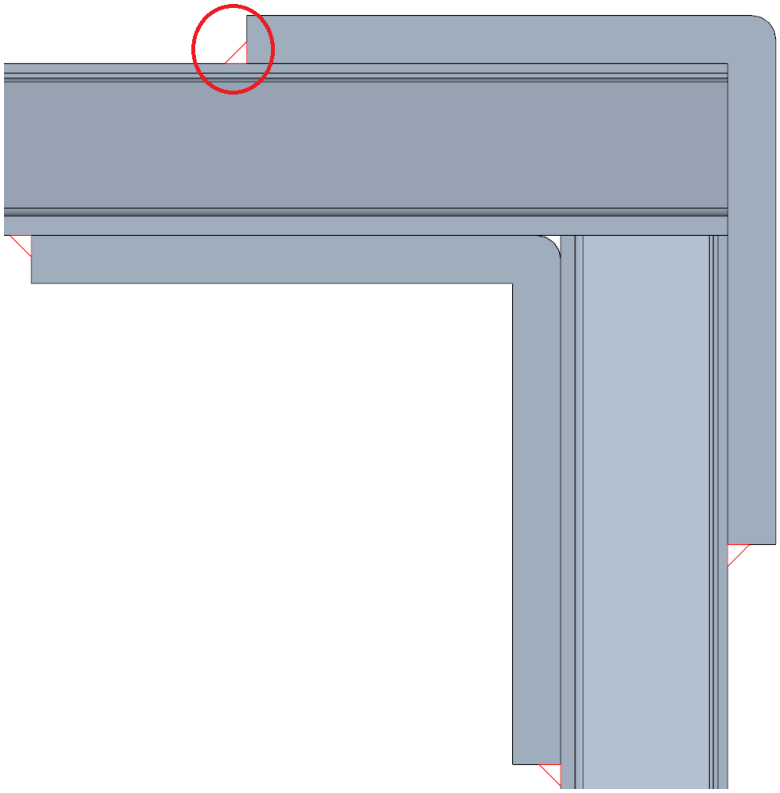

Figure 46. Assembly of the corner joint. Detailed weld model below.

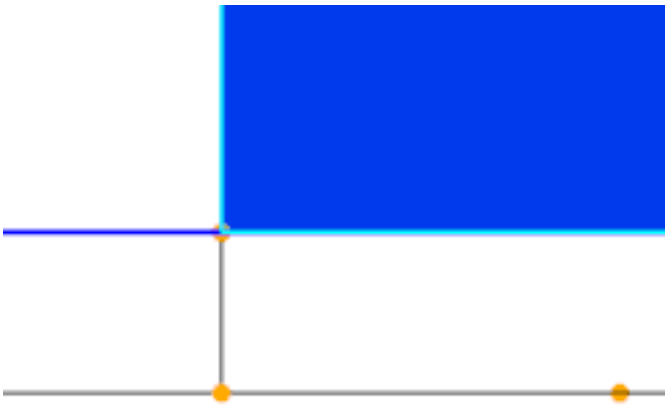

Figure 47. The joint between solid and midsurface shell element in simulation.

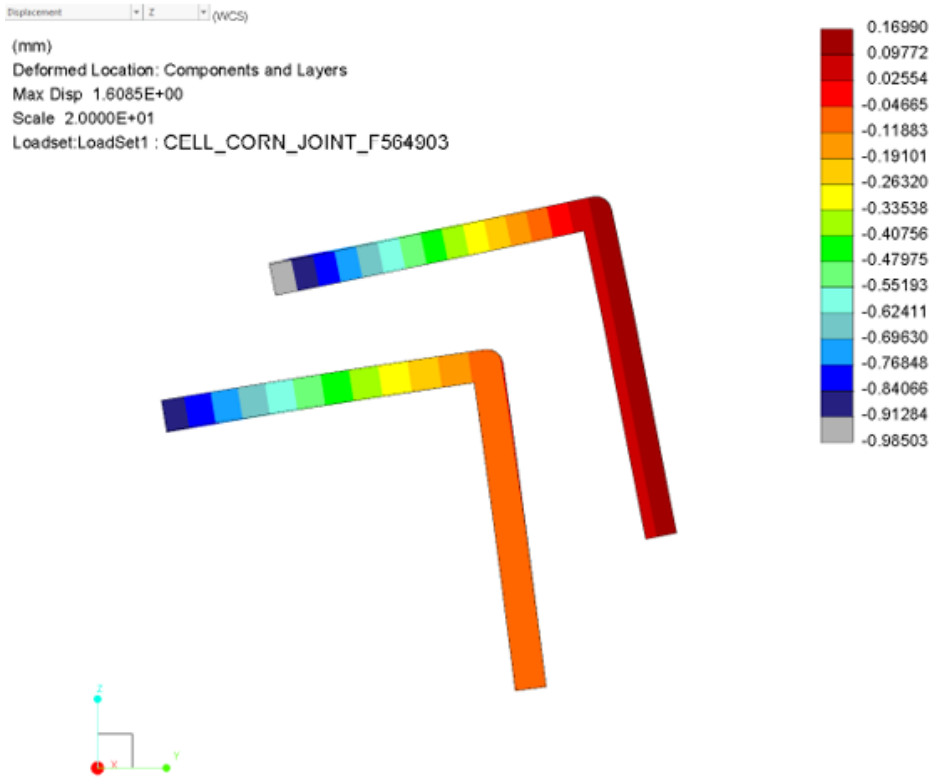

Figure 48. Displacement of the corner joint, scaled 20 times.

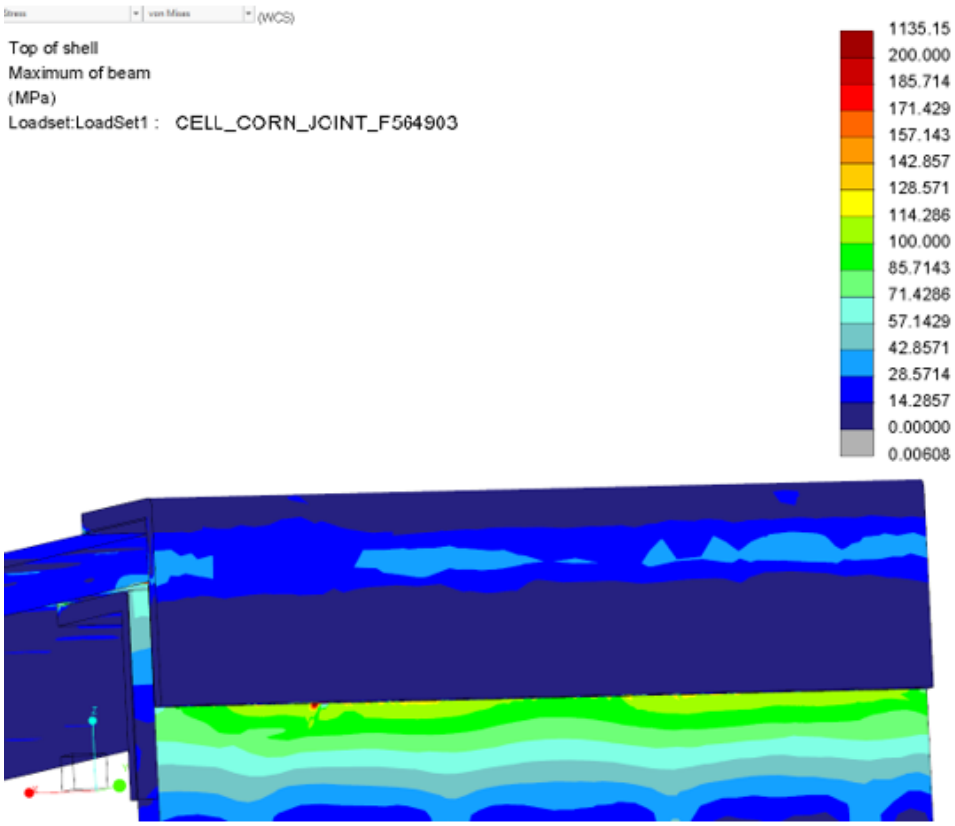

Figure 49. Von Mises stress levels at corner area.

5.2 Joint between panels

Stress levels of RHS pipe was evaluated with boundary conditions illustrated in figure 50. Both ends of the pipe were fixed, and boundary conditions in x and z axis were added at both sides of the pipe. In addition, boundary condition in y-axis was added to L_1 distance of the pipe end. The load $F/2$ was set to point, distance of 1125 mm from the RHS pipe, illustrated in figure 51. The load was set to affect surface regions at both sides of the RHS pipe.

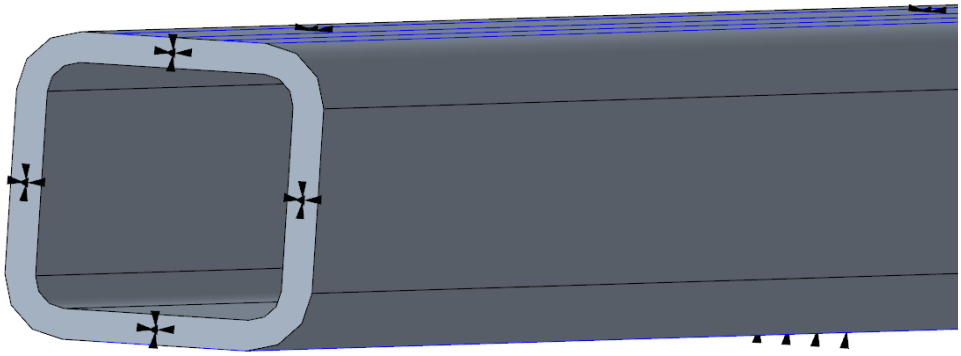

Figure 50. Boundary conditions of the RHS pipe.

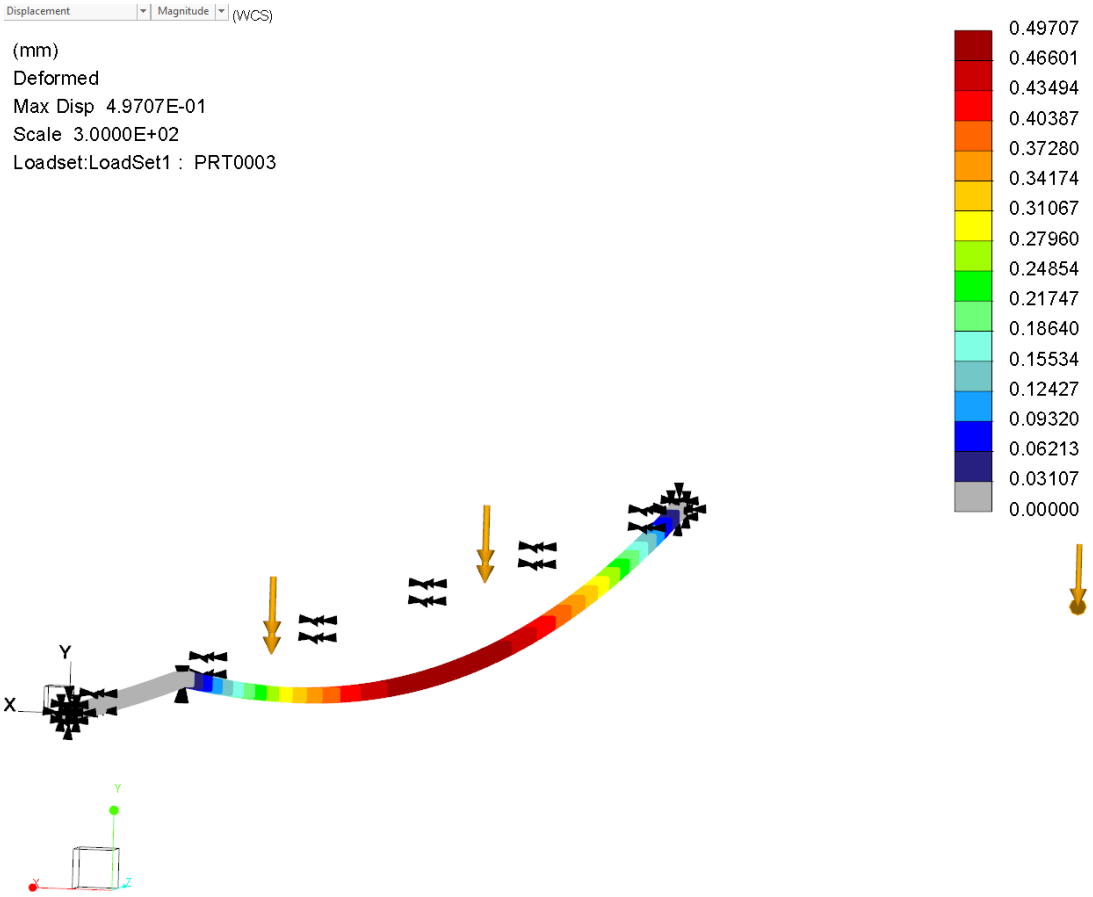

Figure 51. Load affecting to RHS pipe. Color scale of the resulted deflection, scaled 300 times.

The analysis resulted maximum deflection of 0,49 mm. Von Mises stress level of 120 MPa was calculated at the y-axis boundary condition, illustrated in figure 52.

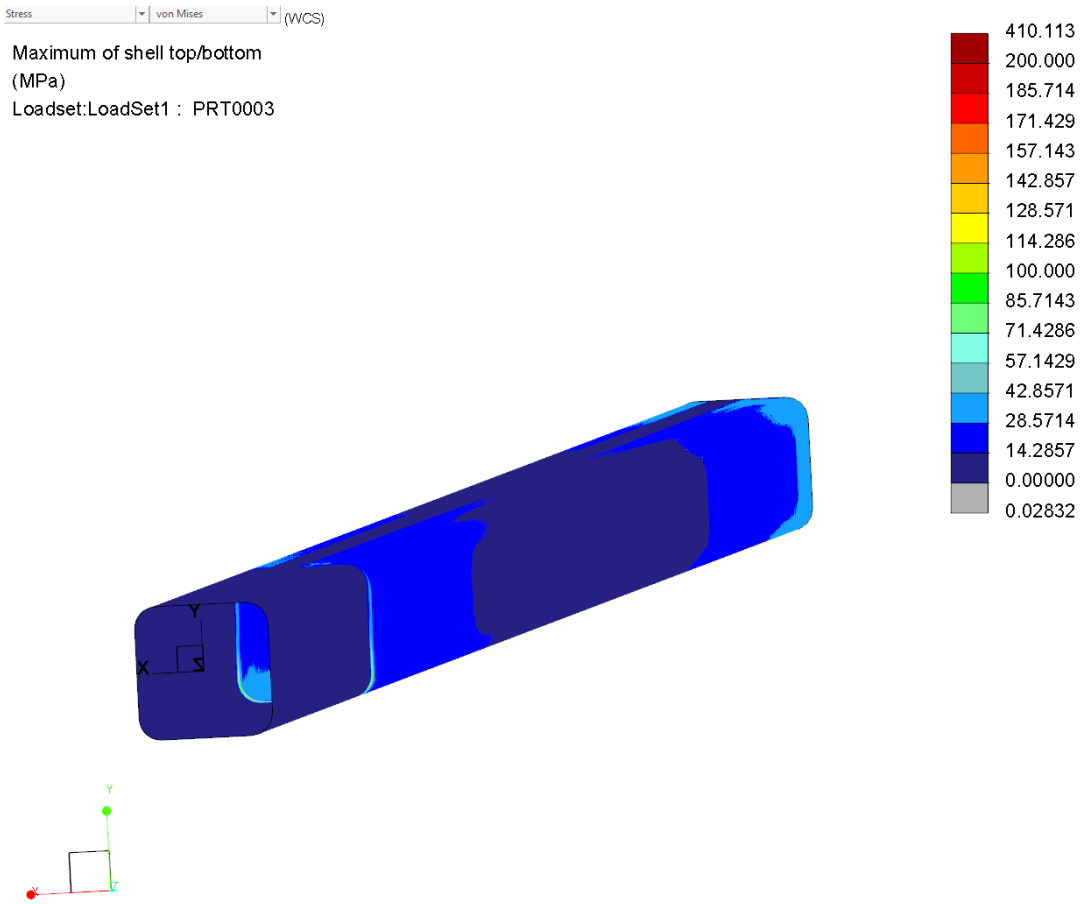

Figure 52. Maximum von Mises stress levels of the RHS pipe.

5.3 Vibration analysis

Vibration analysis was performed for the whole model of sandwich structure, as illustrated in figure 53. Own and additional mass of the loading were taken into account. Fixed boundary condition was set to both ends of the panel, and additional springs were added to model to idealize continuous structure. The spring constant of parallel connected springs were evaluated based on deflection of cross-section to the loading. Table 6 compiles the calculated spring constant and results of vibration analysis. Figures 54 and 55 illustrate the modes of vibration.

Table 6. Calculated spring constant and resulted vibration frequencies.

k [N/mm]	12825/8,8 = 1457/4 = 364
Mode 1 [Hz]	12,8
Mode 2 [Hz]	14,8

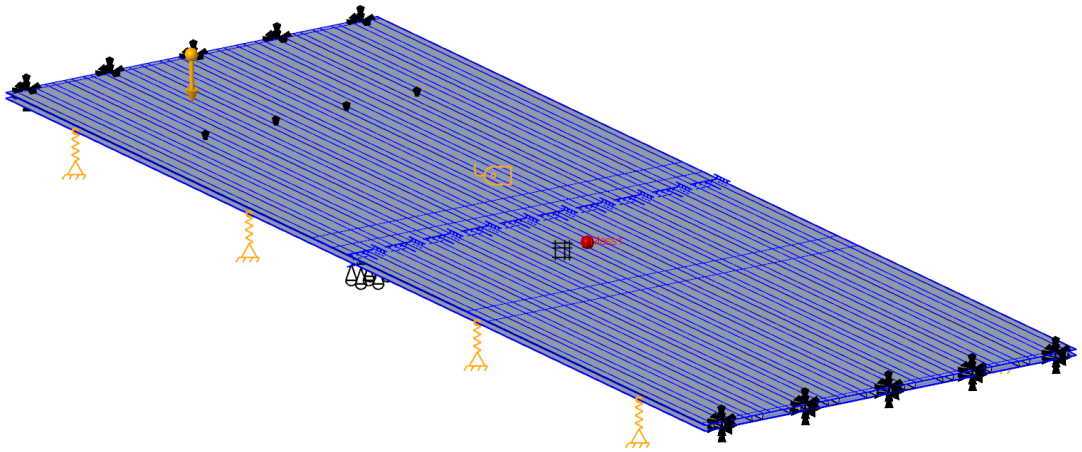

Figure 53. Idealization of continuous structure with added mass.

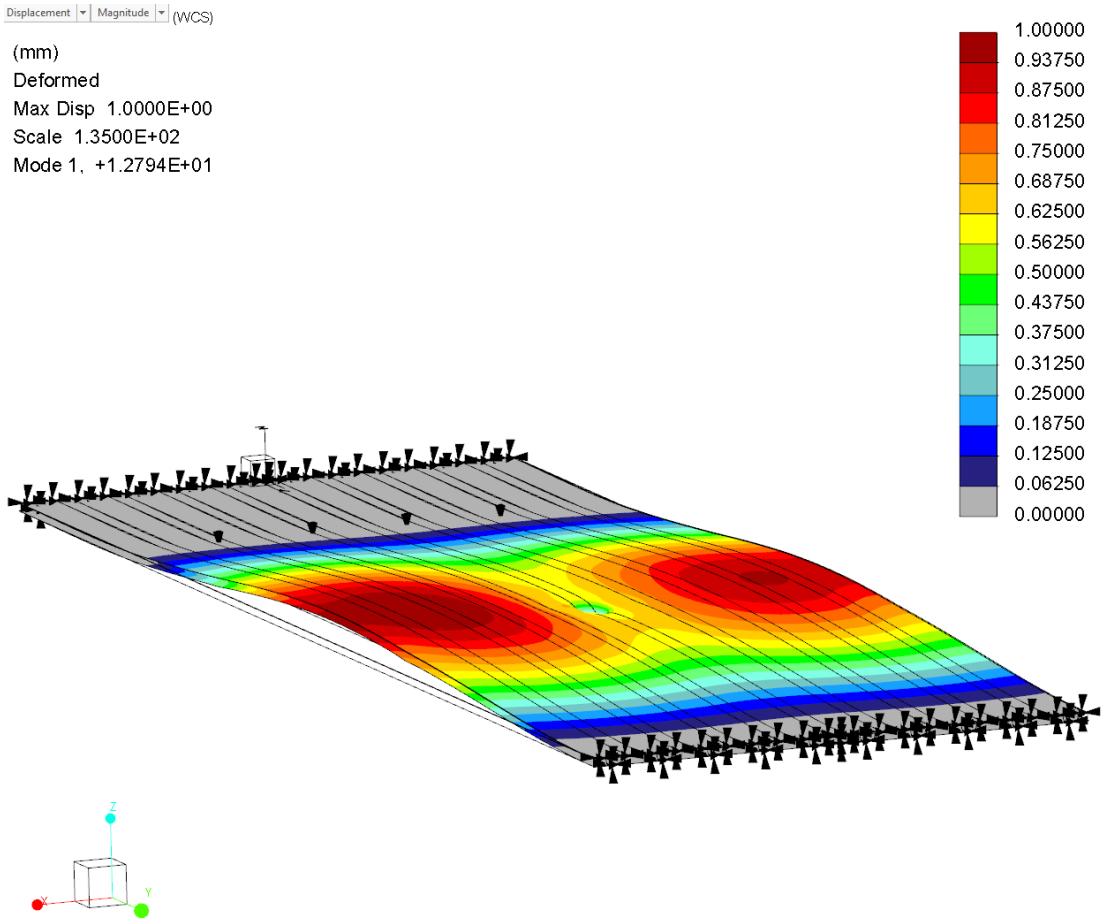

Figure 54. First mode of vibration analysis, scaled 135 times.

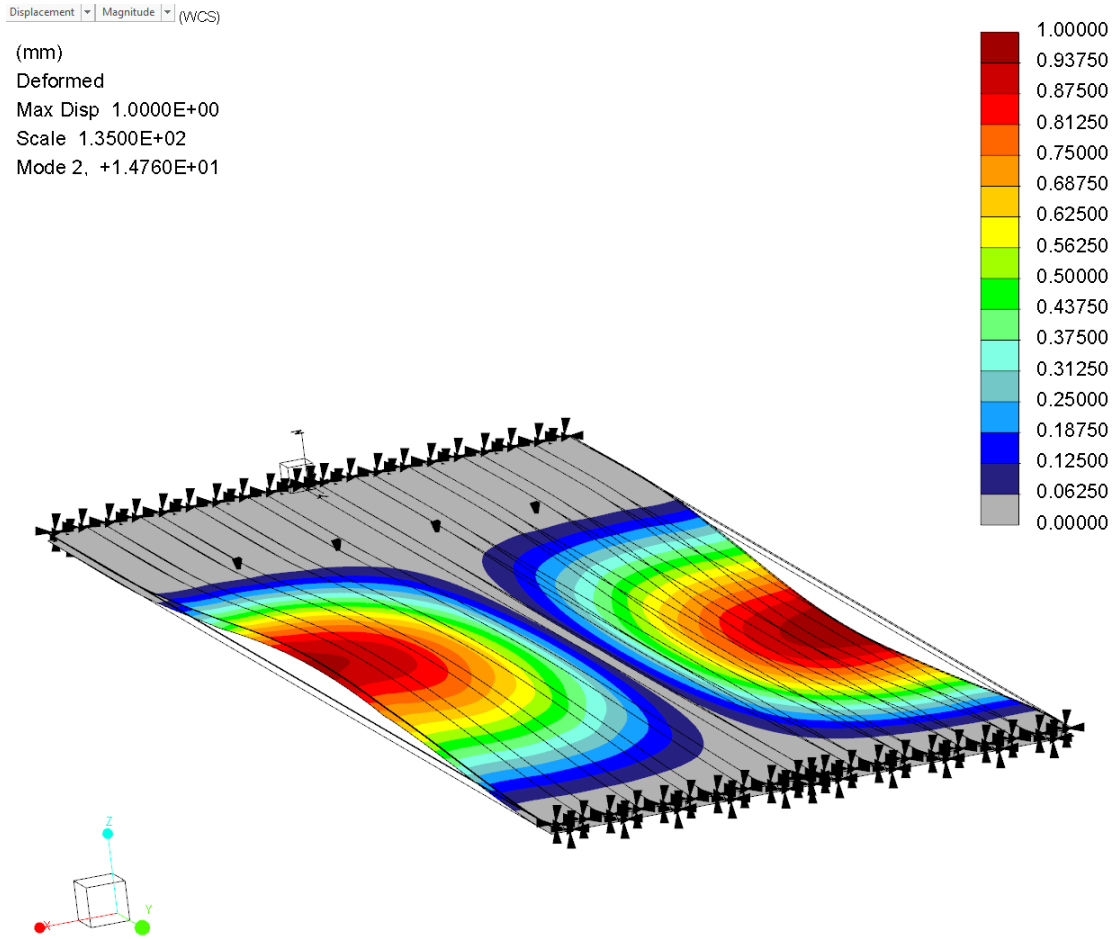

Figure 55. Second mode of vibration analysis, scaled 135 times.

Effect of seismic action was analyzed with lateral shear force added to the one sixth of sandwich panel. The lateral shear force was calculated with the mass of the one sixth of the panel and one sixth of external mass. The external mass was idealized to height of 1 000 mm from the surface of panel and distance of 1 125 mm from the edge of the panel, illustrated in figure 56. The masses were multiplied with lateral acceleration a_s, resulting lateral force of 548 N to the side of the panel and 876 N to the external mass. The main effect of the lateral load can be seen in figure 56.

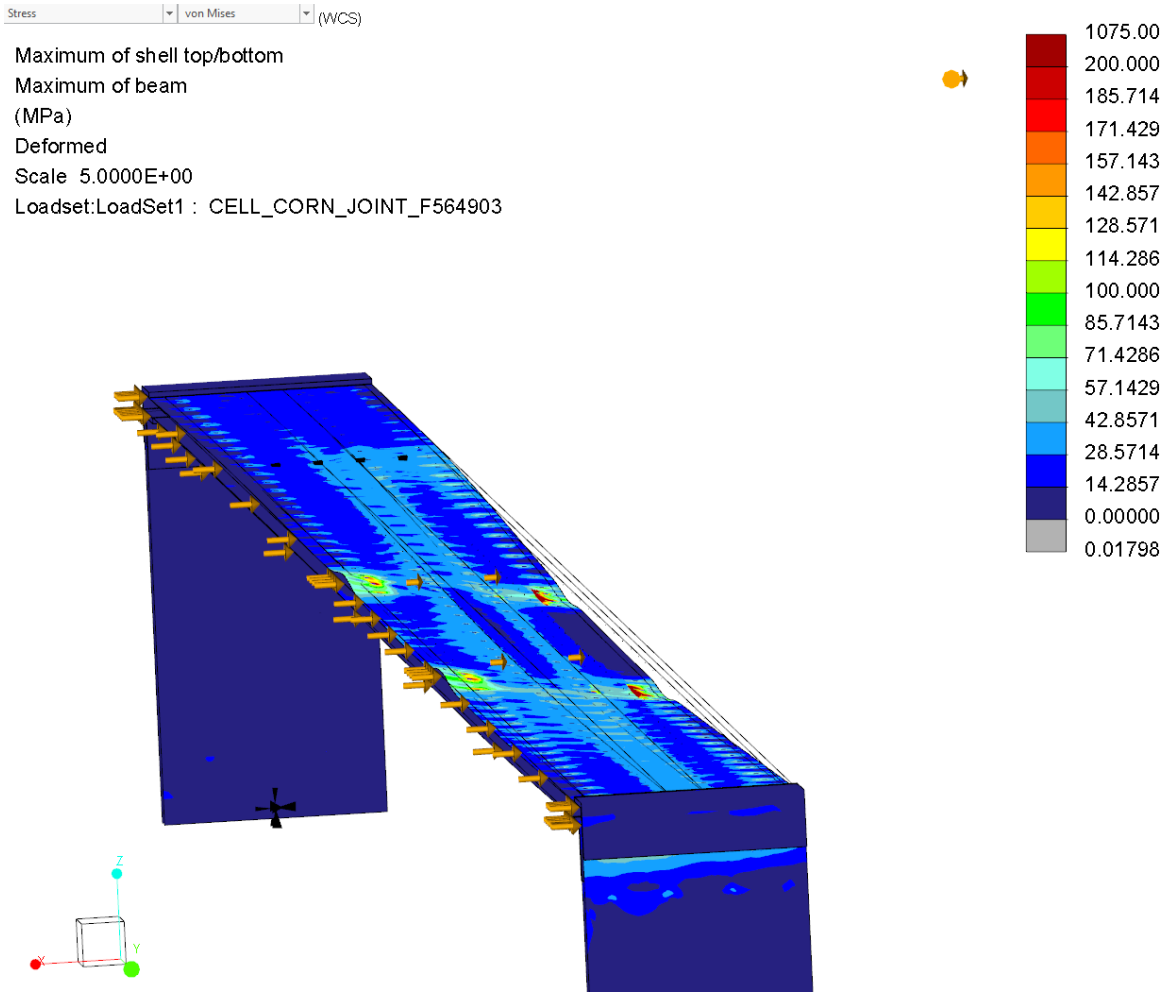

Figure 56. Von Mises stress levels with lateral load, deformations scaled 5 times.

6 CONCLUSIONS

In this thesis, specific failure modes related to sandwich structures were evaluated with analytical calculations and FE-analysis. Chosen details were evaluated as best options to implement the structural requirements with ease of manufacturing. Results of the thesis may be considered reliable, as the results of analytical equations sustain on proven research information and seemed to correlate to FE-analysis with sufficient accuracy. The difference between Excel-based analytical calculation and the results of FE-analysis was 1,8 mm, when deflection was evaluated. The error can be explained with second moment of area calculation in Excel, where bending radius wasn't taken into account. Additionally, the load in the FE-model was divided into two surfaces, affecting to the bending moment diagram of the roof panel. Also, FE-analysis proved the shear buckling and core edge pressure capacity to be in line with analytical calculations. Overall stress levels were moderate, with allowable deflections, if local singularities of sharp corners in the model were not taken into account.

Seismic action increased the stress levels of sandwich panel near spot welds, while stress levels remain below yield strength of material. It can be stated, that the solution has possibility to survive in unexpected conditions, but exploring of the whole structure against seismic action is necessary, when more detailed information is available. Modularity of the sandwich panel can be achieved by cutting the panel in suitable pieces. The inlets should be placed to locations, where stress levels of the panel remain lowest. Inlet placements may be best to do after panel manufacturing, to avoid additional work steps to the production. Bending moment figure should be followed, and airtight connection between sandwich panel and reinforcement is recommended.

As deflection was the main limitation of the structure, cross-section class 3 could not be fully utilized to the yield limit of material. For further investigation, the structure mass could be reduced by using cross-section class 4 limits for face sheets, or by calculating the critical buckling stress limit for section d_3. Critical buckling stress of plate field could be easily added to the Excel sheet. This way, the number of cores could be reduced, which will reduce expenses in sense of material cost, welding and bending. The reduced second moment of area could be replaced by increasing height of the cross-section. The first limitation of core

web height increase is related to shear buckling, but with core thickness of 1 mm the height could be increased to 60 mm. In addition, face sheet point load resistance should be re-evaluated. As mass of the structure changes with the same stiffness properties, it will have effect to the natural frequencies of the structure.

For optimal use of material, core sections b_1 and b_2 should be as narrow as possible. These aspects should be discussed with potential manufacturer, as manufacturing equipment and tolerances define the values. If corrosion resistance plays important role, material selection should be evaluated, as internal corrosion protection is challenging. Cost comparison between corrosion resistant material selection and corrosion protection work should be performed. One option for internal corrosion protection could be airtight structure, but this option sets additional requirement for manufacturing process.

7 SUMMARY

Aim of this thesis was to define suitable metal sandwich structure to be used as load-bearing roof and wall element at elevated temperatures. The thesis focuses on sandwich panel related special issues presented in the literature, and compiles plate field theory and state limit dimensioning presented in Eurocode 3.

As a result, Excel VBA -based solver was created for the V-type core geometry to calculate required cross-section dimensions with minimal use of material, using beam theory. The solver was set to follow cross-section class 3 sheet slenderness ratios. The core geometry was evaluated as best solution, especially for manufacturing. The most efficient way to weld core and face sheets was laser weld.

The solution was evaluated with linear FE-method as well as joints for this panel type. Deflection between analytical calculations and FE-model were consistent with sufficient accuracy. Vibration analysis and lateral seismic action were performed with FE-method also. Based on FE-analysis, the produced solution was stated safe from stability aspect. Material and manufacturing cost could be reduced by optimizing plate field slenderness values that differ from cross-section class 3 method.

LIST OF REFERENCES

Cook, R.D. 1995. Finite element modelling for stress analysis. New York: Wiley. 320 p.

Craig, R. R., Jr. 1981. Structural dynamics: An introduction to computer methods. New York: Wiley. 527 p.

Davies, J.M. 2001. Lightweight sandwich construction. Oxford: Blackwell Science. 370 p.

Jotuni, P., Ryti, H. & Pöyhönen O. 1975. Tekniikan käsikirja: 1, Yleiset perusteet. Jyväskylä: Gummerus. 566 p.

Kujala, P., Romanoff, J., Salminen, A., Varis, J. & Vilpas, M. 2003. Teräksiset kerroslevyrakenteet. Helsinki: Metalliteollisuuden kustannus. 84 p.

Kullaa, J., Leino, T. & Kärnä, T. 1998. Maanjäristyksen kestävät teräsrakenteet. Espoo: Valtion teknillinen tutkimuskeskus. 59 p.

Niemi, E. 2003. Levyrakenteiden suunnittelu. Helsinki: Teknologiainfo Teknova. 136 p.

Nuutinen, J. 1999. Ohutlevyjen liittäminen. Helsinki: Metalliteollisuuden kustannus. 107 p. (MET, Tekninen tiedotus 7/1999.)

Ongelin, P. & Valkonen, I. 2010. Hitsatut profiilit EN 1993 -käsikirja. 3rd edition. Hämeenlinna: Rautaruukki Oyj. 608 p.

Ongelin, P. & Valkonen, I. 2016. Rakenneputket EN 1993 -käsikirja. Hämeenlinna: SSAB Europe Oy. 688 p.

Pennala, E. 1999. Koneiden ja rakenteiden värähtelyt. Helsinki: Otatieto. 314 p.

Pennala, E. 2000. Lujuusopin perusteet. 7th edition. Helsinki: Otatieto. 400 p.

Raute Oyj. 2019. About Raute. [Raute's web-page]. [Referred 4.9.2019]. Available: https://www.raute.com/about-raute

SFS-EN-1990. 2006. Eurocode. Basis of structural design. Helsinki: Finnish standards association SFS. 184 p.

SFS-EN-1993-1-2. 2005. Eurocode 3. Design of steel structures. Part 1-2. General rules. Structural fire design. Helsinki: Finnish standards association SFS. 82 p.

SFS-EN-1993-1-3. 2006. Eurocode 3. Design of steel structures. Part 1-3. General rules. Supplementary rules for cold-formed members and sheeting. Helsinki: Finnish standards association SFS. 130 p.

SFS-EN-1993-1-5. 2006. Eurocode 3. Design of steel structures. Part 1-5. Plated structural elements. Helsinki: Finnish standards association SFS. 55 p.

Teräsrakenneyhdistys. 2013. Teräsrakenteiden maanjäristysmitoitus [verkkodokumentti]. [Viitattu 19.11.2019].
Saatavissa: http://www.terasrakenneyhdistys.fi/document/1/118/19c1dc0/jalkanen_tersrakenteiden_maanjristysmitoitus.pdf

Zenkert, D. (1997). The handbook of sandwich construction. Cradley Heath: Emas Publishing. 442 p.

Bending moment and shear force calculation

Bending moments and shear forces, according to Tekniikan käsikirja pp.53-54

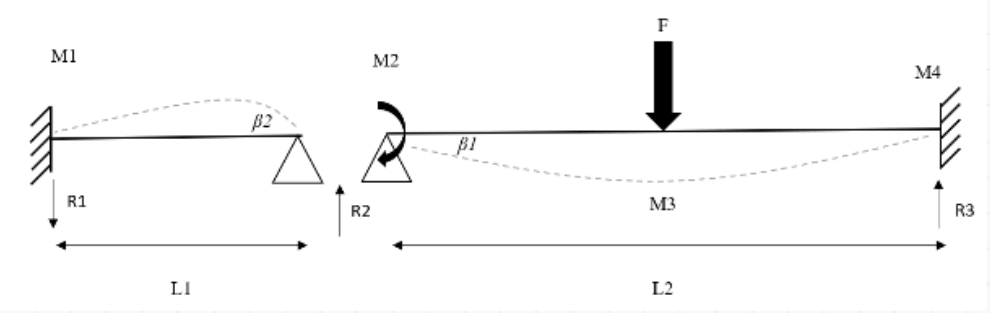

$L1 := 1250 \quad mm$
$L2 := 5522 \quad mm$
$F := 12825 \quad N$

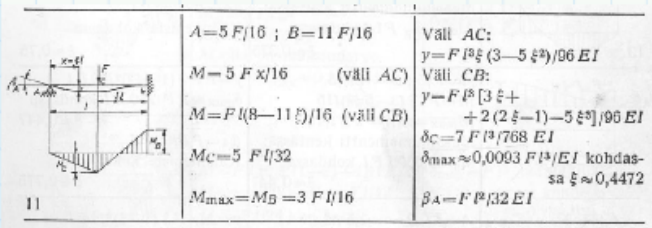

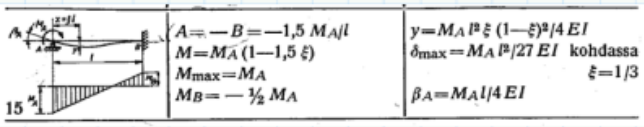

Compatibility condition for yield lines at pin support:

Beeta 1 = Beeta 2

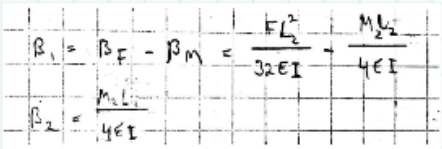

$$M2 := \frac{\frac{F \cdot L2^2}{32}}{\frac{(L1+L2)}{4}} = 7.218 \cdot 10^6 \quad Nmm$$

$$M1 := -0.5 \cdot M2 = -3.609 \cdot 10^6 \quad Nmm$$

$$M3 := \frac{-5 \cdot F \cdot L2}{32} + M2 \cdot (1 - 1.5 \cdot 0.5) = -9.261 \cdot 10^6 \quad Nmm$$

$$M4 := \frac{3 \cdot F \cdot L2}{16} + M2 \cdot (1 - 1.5 \cdot 1) = 9.669 \cdot 10^6 \quad Nmm$$

Reaction forces

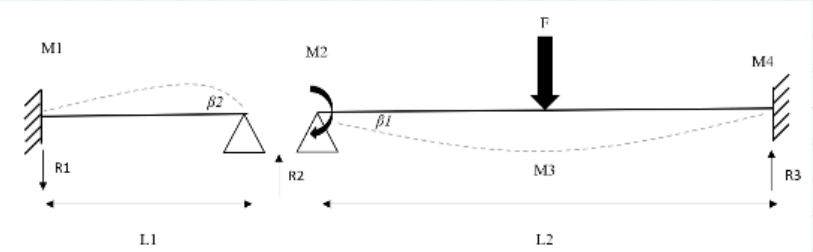

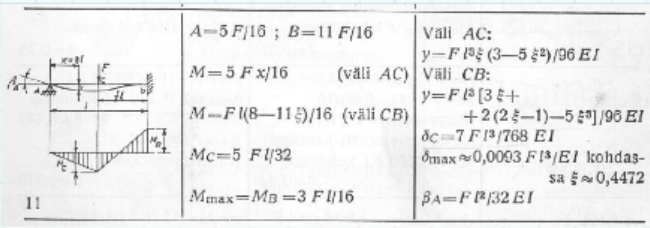

11	$A=5F/16$; $B=11F/16$ $M=5Fx/16$ (väli AC) $M=Fl(8-11\xi)/16$ (väli CB) $M_C=5Fl/32$ $M_{max}=M_B=3Fl/16$	Väli AC: $y=Fl^3\xi(3-5\xi^2)/96EI$ Väli CB: $y=Fl^3[3\xi+2(2\xi-1)-5\xi^3]/96EI$ $\delta_C=7Fl^3/768EI$ $\delta_{max}\approx 0{,}0093Fl^3/EI$ kohdassa $\xi\approx 0{,}4472$ $\beta_A=Fl^2/32EI$

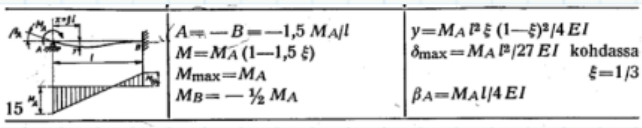

15	$A=-B=-1{,}5M_A/l$ $M=M_A(1-1{,}5\xi)$ $M_{max}=M_A$ $M_B=-\frac{1}{2}M_A$	$y=M_Al^2\xi(1-\xi)^2/4EI$ $\delta_{max}=M_Al^2/27EI$ kohdassa $\xi=1/3$ $\beta_A=M_Al/4EI$

$$R1 := -1.5 \cdot \frac{M2}{L1} = -8.662 \cdot 10^3 \quad N$$

$$R2 := \frac{F}{2} - R1 = 1.507 \cdot 10^4 \quad N$$

$$R3 := \frac{F}{2} = 6.413 \cdot 10^3 \quad N$$

Excel solver

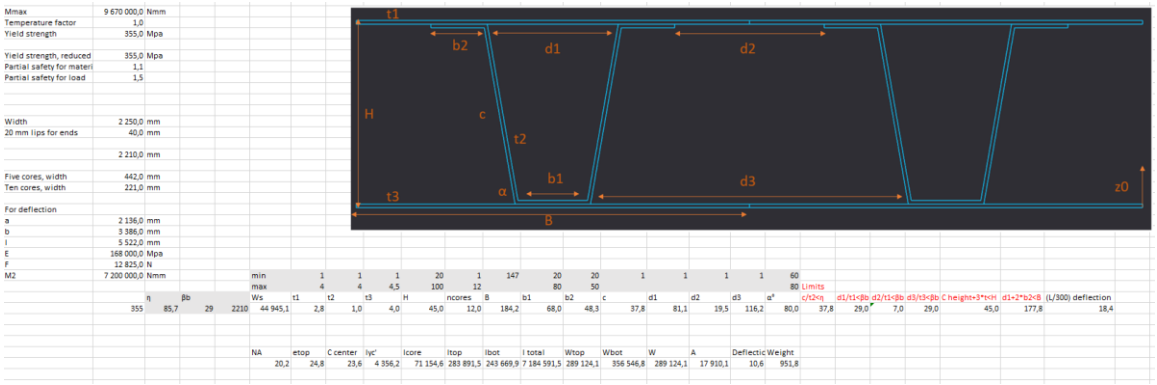

Mmax	9 670 000,0	Nmm
Temperature factor	1,0	
Yield strength	355,0	Mpa
Yield strength, reduced	355,0	Mpa
Partial safety for materi	1,1	
Partial safety for load	1,5	
Width	2 250,0	mm
20 mm lips for ends	40,0	mm
	2 210,0	mm
Five cores, width	442,0	mm
Ten cores, width	221,0	mm
For deflection		
a	2 136,0	mm
b	3 386,0	mm
I	5 522,0	mm
E	168 000,0	Mpa
F	12 825,0	N
M2	7 200 000,0	Nmm

min			1	1	1	20	1	147	20	20	1	1	1	1	60									
max			4	4	4,5	100	12		80	50					80	Limits								
	η	βb			Ws	t1	t2	t3	H	ncores	B	b1	b2	c	d1	d2	d3	α°	c/t2<η	d1/t1<βb	d2/t1<βb	d3/t3<βb	C height=3*t+H	d1+2*b2<B	(L/300) deflection
	355	85,7	29	2210	44 945,1	2,8	1,0	4,0	45,0	12,0	184,2	68,0	48,3	37,8	81,1	19,5	116,2	80,0	37,8	29,0	7,0	29,0	45,0	177,8	18,4

NA	etop	C center	Iyc'	Icore	Itop	Ibot	I total	Wtop	Wbot	W	A	Deflectic	Weight
20,2	24,8	23,6	4 356,2	71 154,6	283 891,5	243 669,9	7 184 591,5	289 124,1	356 546,8	289 124,1	17 910,1	10,6	951,8

```
Sub Cell_PL3()
'
' Cell_PL3 Macro
'

'
    SolverOk SetCell:="$AL$30", MaxMinVal:=2, ValueOf:=0, ByChange:= _
        "$J$30,$K$30,$M$30,$N$30,$S$30,$G$30,$H$30,$I$30", Engine:=1, EngineDesc:= _
        "GRG Nonlinear"
    SolverAdd CellRef:="$AK$30", Relation:=3, FormulaText:="$F$30"
    SolverAdd CellRef:="$AM$30", Relation:=1, FormulaText:="$Z$30"
    SolverAdd CellRef:="$G$30", Relation:=1, FormulaText:="$G$28"
    SolverAdd CellRef:="$G$30", Relation:=3, FormulaText:="$G$27"
    SolverAdd CellRef:="$H$30", Relation:=1, FormulaText:="$H$28"
    SolverAdd CellRef:="$H$30", Relation:=3, FormulaText:="$H$27"
    SolverAdd CellRef:="$I$30", Relation:=1, FormulaText:="$I$28"
    SolverAdd CellRef:="$I$30", Relation:=3, FormulaText:="$I$27"
    SolverAdd CellRef:="$J$30", Relation:=1, FormulaText:="$J$28"
    SolverAdd CellRef:="$J$30", Relation:=3, FormulaText:="$J$27"
    SolverAdd CellRef:="$K$30", Relation:=1, FormulaText:="$K$28"
    SolverAdd CellRef:="$K$30", Relation:=3, FormulaText:="$K$27"
    SolverAdd CellRef:="$K$30", Relation:=4, FormulaText:="integer"
    SolverAdd CellRef:="$L$30", Relation:=3, FormulaText:="$L$27"
    SolverAdd CellRef:="$M$30", Relation:=1, FormulaText:="$M$28"
    SolverAdd CellRef:="$M$30", Relation:=3, FormulaText:="$M$27"
    SolverAdd CellRef:="$N$30", Relation:=1, FormulaText:="$N$28"
    SolverAdd CellRef:="$N$30", Relation:=3, FormulaText:="$N$27"
    SolverAdd CellRef:="$O$30", Relation:=3, FormulaText:="$O$27"
    SolverAdd CellRef:="$P$30", Relation:=3, FormulaText:="$P$27"
    SolverAdd CellRef:="$Q$30", Relation:=3, FormulaText:="$Q$27"
    SolverAdd CellRef:="$R$30", Relation:=3, FormulaText:="$R$27"
    SolverAdd CellRef:="$S$30", Relation:=1, FormulaText:="$S$28"
    SolverAdd CellRef:="$S$30", Relation:=3, FormulaText:="$S$27"
    SolverAdd CellRef:="$T$30", Relation:=1, FormulaText:="$C$30"
    SolverAdd CellRef:="$U$30", Relation:=1, FormulaText:="$D$30"
    SolverAdd CellRef:="$V$30", Relation:=1, FormulaText:="$D$30"
    SolverAdd CellRef:="$W$30", Relation:=1, FormulaText:="$D$30"
    SolverAdd CellRef:="$X$30", Relation:=1, FormulaText:="$J$30"
    SolverAdd CellRef:="$Y$30", Relation:=1, FormulaText:="$L$30"
    SolverOk SetCell:="$AL$30", MaxMinVal:=2, ValueOf:=0, ByChange:= _
        "$J$30,$K$30,$M$30,$N$30,$S$30,$G$30,$H$30,$I$30", Engine:=1, EngineDesc:= _
        "GRG Nonlinear"
    SolverOk SetCell:="$AL$30", MaxMinVal:=2, ValueOf:=0, ByChange:= _
        "$J$30,$K$30,$M$30,$N$30,$S$30,$G$30,$H$30,$I$30", Engine:=1, EngineDesc:= _
        "GRG Nonlinear"
    SolverSolve
End Sub
```

Core edge pressure capacity

Edge pressure capacity according to EN 1993-1-3, pp. 50-52

$r := 1 \quad mm$
$t := 1 \quad mm$
$hw := 38 \quad mm$

$\frac{r}{t} = 1 \qquad \frac{hw}{t} = 38$

$fy := 355 \quad MPa$
$E := 168000 \quad MPa$
$\gamma m1 := 1.1$
$\phi := 80$

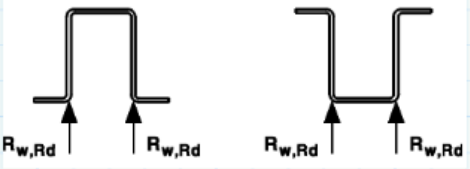

$Ved1 := 8660 \quad N$
$Ved2 := 6340 \quad N$
$\gamma f := 1.5$

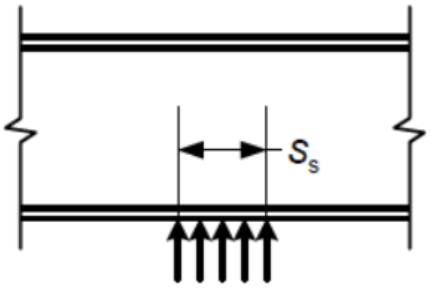

Category 2, support reaction at intermediate support

$$\beta v := \frac{Ved1 - Ved2}{Ved1 + Ved2} = 0.155$$

$la := 40 \quad mm$
$\alpha := 0.115$

$$Rw.Rd := \alpha \cdot t^2 \cdot \sqrt{fy \cdot E} \cdot \left(1 - 0.1 \cdot \sqrt{\frac{r}{t}}\right) \cdot \left(0.5 + \sqrt{0.02 \cdot \frac{la}{t}}\right) \cdot \frac{\left(2.4 + \left(\frac{\phi}{90}\right)^2\right)}{\gamma m1} = 3.232 \cdot 10^3 \quad N$$

$\gamma f \cdot Ved1 = 1.299 \cdot 10^4 \quad N \quad < \quad Rw.Rd \cdot 24 = 7.758 \cdot 10^4 \quad N \quad$ -> ok

Shear lag effect

Effective width, shear lag according to EN 1993-1-5, pp. 9-11

Overall shear lag, width of 2250 mm

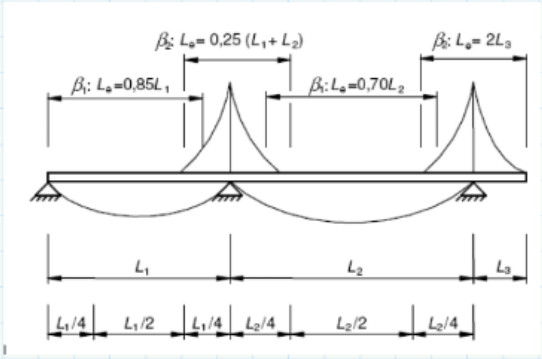

$$b0 := \frac{2250}{2} = 1.125 \cdot 10^3\ mm$$

$$Le := 2 \cdot 1420 = 2.84 \cdot 10^3 \quad mm$$

$$\frac{Le}{50} = 56.8 \quad mm$$

$$t := 3\ mm$$

$$Asl := 6 \cdot 198 \quad mm^2$$

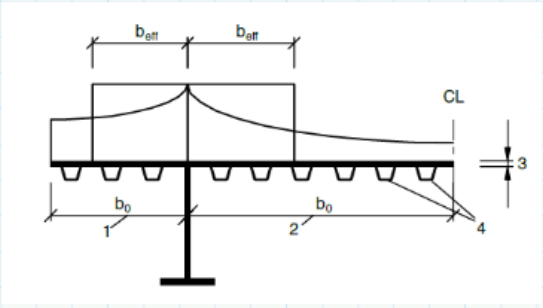

$$\alpha := \sqrt{1 + \frac{Asl}{b0 \cdot t}} = 1.163$$

$$\kappa := \alpha \cdot \frac{b0}{Le} = 0.461$$

$$\beta := \frac{1}{1 + 6 \cdot \left(\kappa - \frac{1}{2500 \cdot \kappa}\right) + 1.6 \cdot \kappa^2} = 0.244$$

κ	Verification	β – value
$\kappa \le 0{,}02$		$\beta = 1{,}0$
$0{,}02 < \kappa \le 0{,}70$	sagging bending	$\beta = \beta_1 = \frac{1}{1 + 6{,}4\,\kappa^2}$
	hogging bending	$\beta = \beta_2 = \frac{1}{1 + 6{,}0\left(\kappa - \frac{1}{2500\,\kappa}\right) + 1{,}6\,\kappa^2}$
$> 0{,}70$	sagging bending	$\beta = \beta_1 = \frac{1}{5{,}9\,\kappa}$
	hogging bending	$\beta = \beta_2 = \frac{1}{8{,}6\,\kappa}$
all κ	end support	$\beta_0 = (0{,}55 + 0{,}025/\kappa)\,\beta_1$, but $\beta_0 < \beta$
all κ	Cantilever	$\beta = \beta_c$ at support and at the end

$\kappa = \alpha_0\, b_e / J_c$ with $\alpha_0 = \sqrt{1 + \frac{A_{sl}}{b_e t}}$

in which A_{sl} is the area of all longitudinal stiffeners within the width b_e and other symbols are as defined in Figure 3.1 and Figure 3.2.

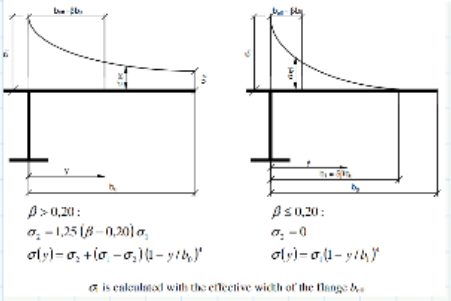

$beff := 2 \cdot \beta \cdot b0 = 549.072\ \ mm$ for whole cross-section

Nominal stress of face sheet

$$M := 9.67 \cdot 10^6 \quad Nmm$$
$$c := 25 \quad mm$$
$$I := 72 \cdot 10^5 \quad mm^4$$

$$\sigma max := \frac{M \cdot c}{I} = 33.576 \quad MPa$$

$$\sigma 1 := \sigma max \cdot \frac{b0}{beff} = 68.795 \quad MPa$$

$$\sigma 2 := 1.25 \cdot (\beta - 0.2) \cdot \sigma 1 = 3.786\ MPa$$

Buckling under shear stress

Buckling under shear stress

$hw := 38 \quad mm$

$tw := 1 \quad mm$

$fy := 355 \quad MPa$

$\eta := 1.2$

$$\frac{hw}{tw} = 38 \quad < \quad \frac{72 \cdot 0.85 \cdot \sqrt{\frac{235}{fy}}}{1.2} = 41.494$$

No need to check the critical buckling under shear stress.

Dimensioning of the corner joint

Dimensioning of the corner joint, according to Pennala 2003, p.106

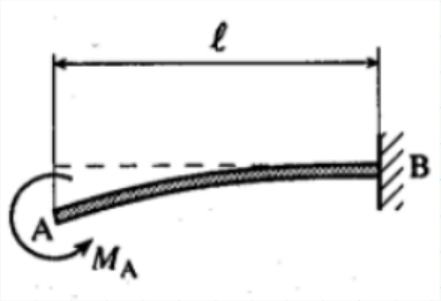

$v := 1$ mm
$M := 9.67 \cdot 10^6$ Nmm
$l := 100$ mm
$b := 2250$ mm
$E := 168000$ MPa

$$h := \sqrt[3]{\frac{12 \cdot M \cdot l^2}{2 \cdot E \cdot v \cdot b}} = 11.535 \quad mm$$

Dimensioning of the weld, EN 1993-1-3

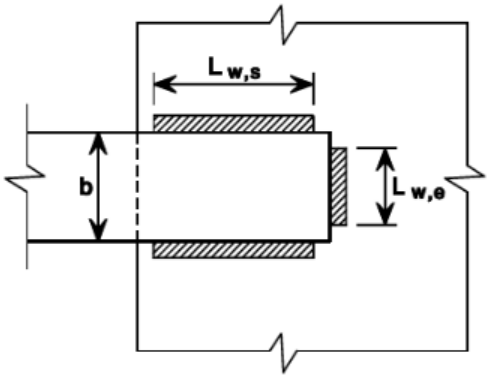

$t := 3$ mm
$Lwe := 2250$ mm
$b := 2250$ mm
$fu := 510$ MPa
$\gamma m2 := 1.25$

$\sigma fe := 69$ MPa overall shear lag taken into account

$$Fed := \sigma fe \cdot b \cdot t = 4.658 \cdot 10^5 \quad < \quad FwRd := t \cdot Lwe \cdot \left(1 - 0.3 \cdot \frac{Lwe}{b}\right) \cdot \frac{fu}{\gamma m2} = 1.928 \cdot 10^6 \quad N$$

-> a 3 mm ok

Shear resistance of the attachment joint

Joint between panels, 40x40x3 RHS pipe, according to Ongelin et al. 2016, pp.102 & 540

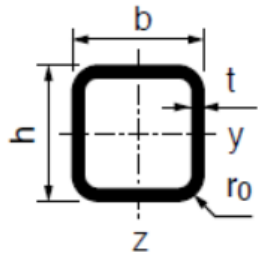

$\gamma f := 1.5$
$Vmax := 8660 \quad N$
$\gamma m0 := 1$
$fy := 355$

$h := 40 \quad mm$
$b := 40 \quad mm$
$t := 3 \quad mm$

$A := 4.21 \cdot 10^2 \quad mm^2$
$\varepsilon := 0.7$
$\eta := 1$

$\frac{h}{t} = 13.333 < \frac{72 \cdot \varepsilon}{\eta} + 3 = 53.4$ Only plastic shear strenght required

$Av := A \cdot \frac{h}{b+h} = 210.5 \quad mm^2$

$Vmax \cdot \gamma f = 1.299 \cdot 10^4 \quad N \quad < VplRd := Av \cdot \frac{\frac{fy}{\sqrt{3}}}{\gamma m0} = 4.314 \cdot 10^4 \quad N$ -> OK

Attachment weld, EN 1993-1-3

$\gamma m2 := 1.25$
$fu := 510$
$t := 3$
$b := 30$

$FwRd := 0.45 \cdot t \cdot b \cdot \frac{fu}{\gamma m2} = 1.652 \cdot 10^4 \quad N$

$Vmax \cdot \gamma f = 1.299 \cdot 10^4 \quad N < \quad 2 \cdot FwRd = 3.305 \cdot 10^4 \quad N$ -> a=3 ok